Remote Sensing of Environment 265 (2021) 112648

Contents lists available at ScienceDirect

Remote Sensing of Environment

journal homepage: www.elsevier.com/locate/rse

# Monitoring temperate forest degradation on Google Earth Engine using Landsat time series analysis

Shijuan Chen [a,*], Curtis E. Woodcock [a], Eric L. Bullock [b], Paulo Arévalo [a], Paata Torchinava [c], Siqi Peng [a], Pontus Olofsson [a]

[a] Department of Earth and Environment, Boston University, 685 Commonwealth Avenue, Boston, MA 02215, USA
[b] US Forest Service, Rocky Mountain Research Station, Ogden, UT 84401, USA
[c] Department of Biodiversity and Forestry, Ministry of Environmental Protection and Agriculture of Georgia, Tbilisi, Georgia

ARTICLE INFO

Edited by: Marie Weiss

*Keywords:*
Forest degradation
Deforestation
Disturbance
Landsat
Google Earth Engine
CCDC-SMA
Time series analysis
Change detection
Area estimation

ABSTRACT

Current estimates of forest degradation are associated with large uncertainties. However, recent advancements in the availability of remote sensing data (e.g., the free data policies of the Landsat and Sentinel Programs) and cloud computing platforms (e.g., Google Earth Engine (GEE)) provide new opportunities for monitoring forest degradation. Several recent studies focus on monitoring forest degradation in the tropics, particularly the Amazon, but there are less studies of temperate forest degradation. Compared to the Amazon, temperate forests have more seasonality, which complicates satellite-based monitoring. Here, we present an approach, Continuous Change Detection and Classification - Spectral Mixture Analysis (CCDC-SMA), that combines time series analysis and spectral mixture analysis running on GEE for monitoring abrupt and gradual forest degradation in temperate regions. We used this approach to monitor forest degradation and deforestation from 1987 to 2019 in the country of Georgia. Reference conditions were observed at sample locations selected under stratified random sampling for area estimation and accuracy assessment. The overall accuracy of our map was 91%. The user's accuracy and producer's accuracy of the forest degradation class were 69% and 83%, respectively. The sampling-based area estimate with 95% confidence intervals of forest degradation was 3541 ± 556 $km^2$ (11% of the forest area in 1987), which was significantly larger than the area estimate of deforestation, 158 ± 98 $km^2$. Our approach successfully mapped forest degradation and estimated the area of forest degradation in Georgia with small uncertainty, which earlier studies failed to estimate.

## 1. Introduction

Definitions of forest degradation vary in the literature (Simula, 2009). For example, Food and Agriculture Organization (FAO)'s definition of forest degradation emphasizes the reduction of the capability of forests to provide goods and services, including both anthropogenic and natural disturbances (FAO, 2012). Intergovernmental Panel on Climate Change (IPCC)'s definition, however, focuses on carbon loss and constrains forest degradation to human activities (IPCC, 2003). Definitions of forest degradation in other international or national organizations can vary. Based on the existing definitions of forest degradation and the capability of remote sensing, forest degradation in this study is defined as *forests that experienced loss of tree cover due to anthropogenic or natural causes but remain as forest*. Forest is defined as *places with tree cover greater than 10%, excluding orchards*, and deforestation as *conversion from forest to non-forest*. Forest disturbance includes forest degradation and deforestation.

The issue of forest degradation is gaining attention in the scientific community, since carbon emissions from forest degradation are potentially substantial. FAO (2015) and Federici et al. (2015) estimated that global emissions from forest degradation have increased recently and contributed about 25% of the net $CO_2$ emissions from forests. Pearson et al. (2017) found that emissions from forest degradation were higher than those from deforestation in 28 of 74 countries. Baccini et al. (2017) found that carbon loss from forest degradation, defined as reductions in carbon density within standing forests, accounted for 69% of the overall

* Corresponding author.
*E-mail addresses:* shijuan@bu.edu (S. Chen), curtis@bu.edu (C.E. Woodcock), eric.bullock@usda.gov (E.L. Bullock), parevalo@bu.edu (P. Arévalo), bestqiqi@bu.edu (S. Peng), olofsson@bu.edu (P. Olofsson).

https://doi.org/10.1016/j.rse.2021.112648
Received 10 March 2021; Received in revised form 25 July 2021; Accepted 10 August 2021
Available online 27 August 2021

loss from forest degradation and deforestation in the tropics.

The estimated extent and rate of forest degradation have traditionally been associated with large uncertainties with the result that the impact of forest degradation on terrestrial carbon dynamics is poorly understood (FAO, 2015; Federici et al., 2015; Pearson et al., 2017). However, the situation is changing. Recent advancements, including the open data policy (Woodcock et al., 2008), global consolidation of Landsat satellite data (Wulder et al., 2016), cloud computing platforms (Gorelick et al., 2017), the development of time series-based approaches (Kennedy et al., 2010; Verbesselt et al., 2010; Kennedy et al., 2014; Bullock et al., 2020a) and the combined use of sampling techniques and remote sensing (Olofsson et al., 2013; Olofsson et al., 2014), have increased our capability of monitoring and estimating the extent of forest degradation (Mitchell et al., 2017; Bullock et al., 2020b; Quintano et al., 2013). Recent studies using these new advancements show that the extent and rate of forest degradation have been previously underestimated. For example, Bullock et al. (2020b) showed that when considering forest degradation, the area of forest disturbance in the Amazon Ecoregion since 1995 was 60% higher than previously estimated. Matricardi et al. (2020) also found that the extent and rate of forest degradation surpassed that of deforestation in Brazilian Amazon from 1992 to 2014.

Despite an increased focus, forest degradation remains understudied in many parts of the world. In the 2020 Global Forest Resource Assessment by FAO (2020a), only 58 countries reported on forest degradation, representing only 38% of global forest area. In Europe, only 7 countries reported on forest degradation. Furthermore, most studies of forest degradation from the last decade are in the tropics (e.g., Rappaport et al., 2018; Souza et al., 2013; Miettinen et al., 2014; Bullock et al., 2020b; Matricardi et al., 2020). This is partly because forest degradation in the tropics is a more severe issue than in temperate regions. While forest degradation in the tropics is important due to the associated impacts on carbon dynamics, biodiversity, and local climate (Herold et al., 2011), it is likely that newly discovered patterns and dynamics of forest degradation are not confined to the tropics.

Temperate forests, roughly defined as forests located in the temperate zone between 35- and 50-degree latitudes both north and south, represent a wider range of biomes than tropical forests (Strahler, 2011) and account for 16% of the global forest area (FAO, 2020b). In the 2020 Global Forest Resource Assessment (FAO, 2020b), only 15% of the total forest area of countries in temperate regions reported on forest degradation, as compared to 72% in the tropics. One reason why fewer countries in temperate regions reported forest degradation is because forest degradation is not a major problem in these countries. Another reason is that national forest inventories in some temperate countries, like the country of Georgia, are either out of date or did not include forest degradation. Compared to the tropics, degraded temperate forests recover more slowly due to climate constraints. Also, regardless of biome, forest degradation is always associated with environmental consequences, such as carbon emissions, soil erosion, water quality decline, and loss of wildlife habitat.

Due to the variety of the biomes and forest definitions, characterizing change in temperate forest extent and condition is challenging. The difficulty is highlighted by the different estimated trends in temperate forest area between the Forest Resource Assessments (FAO, 2015) which suggests an increase based on self-reported national inventories and remote sensing-based studies (FAO and JRC, 2012; Hansen et al., 2013) that have found that the area of temperate forest is declining in many parts of the world. Recent research even suggests that forest harvest and biomass loss have accelerated considerably across Europe in the last few years (Ceccherini et al., 2020). Compared with tropical forests, temperate forests exhibit different phenology and reflectance characteristics, and it remains an open question if approaches developed for monitoring tropical forest degradation will also work in temperate forests. One example of the difficulty associated with mapping forest degradation in temperate forests is presented in Olofsson et al. (2010), who attempted to map forest changes in the country of Georgia after the collapse of the Soviet Union. Most of the forest disturbance in Georgia was degradation rather than complete forest cover loss, which traditional approaches to remote sensing-based change detection failed to map. The failure was evident by large map errors, and a margin of error of almost 100% of the area estimate of forest disturbance (Olofsson et al., 2010). The same approach applied in neighboring countries, with less forest degradation and more complete forest cover loss, yielded substantially more accurate results (Kuemmerle et al., 2011; Olofsson et al., 2011). Although there are a number of studies on land cover and land use change in Eastern Europe (Lewińska et al., 2020; Baumann et al., 2012; Potapov et al., 2015), we are unaware of efforts to monitor forest degradation in the Caucasus region (Georgia, Armenia, and Azerbaijan) using remote sensing since Olofsson et al. (2010), and the country of Georgia has no reliable estimate of the area affected by forest degradation.

There are several dimensions of complexity to monitoring forest degradation. First, area estimates of forest degradation in the literature vary partly due to different definitions of forest degradation and forestland (Simula, 2009; FAO, 2012; IPCC, 2003). The spatial and temporal scale associated with different definitions may also lead to inconsistent results. Second, forest degradation may not result in complete land cover change but sub-pixel canopy loss that triggers only subtle changes in spectral reflectance. In Georgia, most forest disturbances do not result in complete land cover change, and detecting such subtle changes in satellite imagery is inherently difficult. Third, forest degradation can be either an abrupt event or a gradual process, or both. For example, illegal logging may initially be an abrupt degradation followed by gradual degradation as extraction of individual tree continues. Monitoring combinations of abrupt and gradual degradation processes are difficult and understudied (Vogelmann et al., 2016). Fourth, separating forest degradation from natural intra-annual variability is challenging, particularly in deciduous forests.

The objectives of our study are: (1) to develop an approach to monitor forest degradation in temperate regions and (2) to map forest degradation and estimate the area of forest degradation in Georgia from 1987 to 2019. Here, we developed an approach, Continuous Change Detection and Classification - Spectral Mixture Analysis (CCDC-SMA), which combines recent advancements in remote sensing for monitoring degradation in temperate forests, including spectral mixture analysis (SMA) (Souza et al., 2005; Souza et al., 2013), Continuous Change Detection and Classification (CCDC) (Zhu and Woodcock, 2014b) and COntinuous DEgradation Detection (CODED) (Bullock et al., 2020a) algorithms. CCDC-SMA can monitor both abrupt and gradual forest degradation and runs on Google Earth Engine (GEE), which is easy to adjust and apply to other regions.

## 2. Study area

Our study area (Fig. 1) is the country of Georgia. Georgia is rich in forests, with more than 3 million hectares, or about 40% of the country's total area (Forestry Department at the Georgian Ministry of Environment and Agriculture, 2006; FAO, 2019). Georgia's forests are rich in biodiversity since Georgia has a wide variety of climates and topography despite being a relatively small country. The Caucasus Ecoregion, where Georgia is located at, is among the top 25 richest and most endangered biological hotspots in the world and is identified as one of the "Global 200 Ecoregions" by World Wide Fund for Nature (WWF) (Krever et al., 2001). Forest degradation is a major threat to biodiversity of the Caucasus Ecoregion (Krever et al., 2001).

Georgia was a republic in the Soviet Union and gained independence in 1991. Since independence, the frequent changes in administrative organizations and the socio-economic turmoil in Georgia, such as the Rose Revolution in 2003 and the Russo-Georgian War in 2008, have disrupted forest management (Zeidler and Schachtschabel, 2016). Due to poor forest management, Georgia's forests have been under pressure

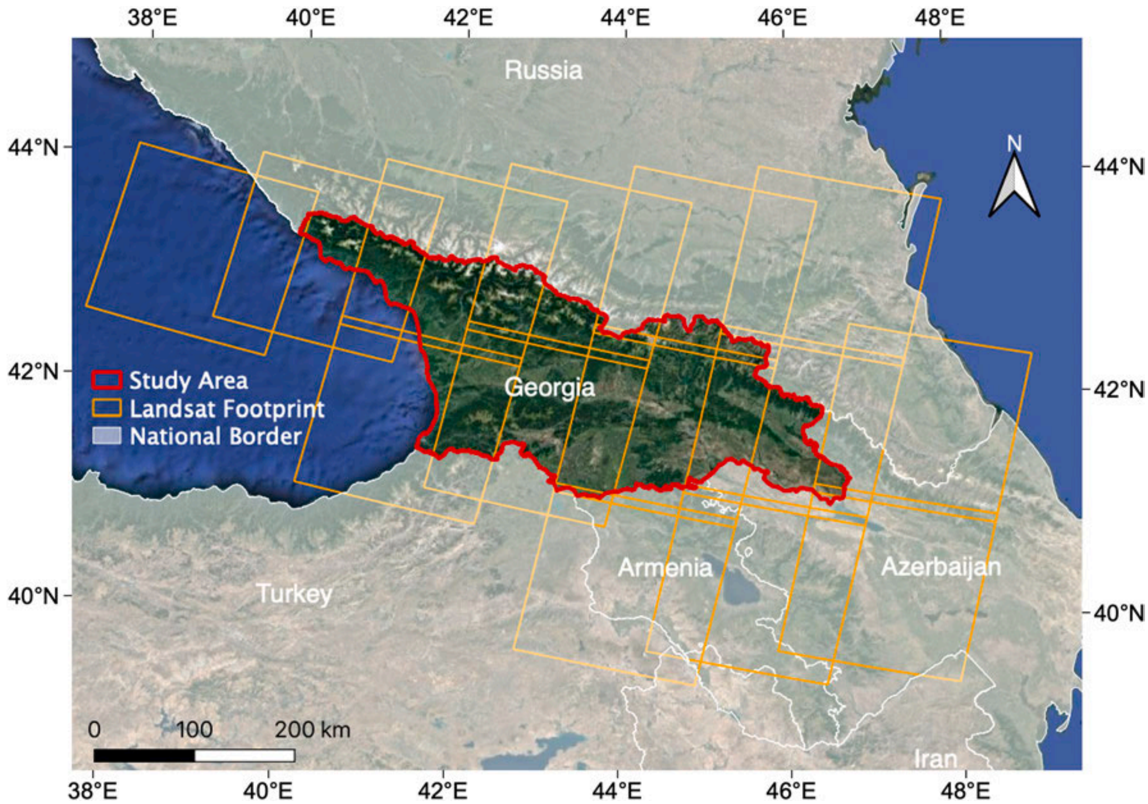


**Fig. 1.** Study area, the country of Georgia.

from illegal and unsustainable logging (Gutman and Radeloff, 2016; FAO, 2019; Olofsson et al., 2010). There were two primary causes of forest degradation in Georgia after independence. First, timber imports from Russia stopped after independence, which led to increased logging for timber (Gutman and Radeloff, 2016). Second, the reduction of energy imports from Russia resulted in intensive logging activities for fuelwood, as rural residents lacked affordable alternatives to wood as a heating fuel (Gutman and Radeloff, 2016). While still unclear, forest degradation due to harvest appears to be the main carbon-emitting activity on the land surface as opposed to deforestation and other land use changes (FAO, 2019; Matcharashvili, 2012; Olofsson et al., 2010; Bziava and Gubeladze, 2003; Dalgleish et al., 2007). It was estimated that about 2.7–3.0 million $m^3$ of wood were removed from Georgia's forest in 2014 and 75% of the removals were illegal logging (Garforth et al., 2016; World Bank, 2020). Although illegal logging is a major threat to Georgia's forests, the official statistics of illegal logging in Georgia are inaccurate and likely underestimate the actual volume (Zeidler and Schachtschabel, 2016). Georgia has no reliable and comprehensive national forest inventory of forest degradation yet, which necessitates the use of remote sensing to monitor forest degradation. We are not aware of remote sensing-based studies of forest degradation in Georgia since 2010 (Olofsson et al., 2010). Thus, the extent and rates of deforestation and forest degradation in Georgia during the last 30 years remain unclear (FAO, 2019; FAO, 2020a).

## 3. Method

### 3.1. Overview

We used all available Landsat Collection 1 surface reflectance data for our analysis and Google Earth Engine as the data processing platform. Fourteen Landsat scenes are required to cover Georgia (Fig. 1), and the study period was defined as 1987–2019 to include the end of the Soviet era and the subsequent civil war in 1991–1992. We tested harmonization (Roy et al., 2016a) and bidirectional reflectance distribution function (BRDF) - correction (Roy et al., 2016b) of Landsat time series data. Although harmonization and BRDF-correction are useful in other contexts, we found that these two steps did not improve our results. Thus, we used Landsat time series without harmonization and BRDF-correction because it reduces the computational burden and simplifies the application of the methodology. There are four major parts of our method. The first part is land cover classification (Section 3.2) since mapping forest degradation requires accurate maps of forest as a starting point. The land cover classification was based on CCDC algorithm using all available Landsat data with the original spectral bands (Zhu et al., 2012; Zhu and Woodcock, 2014b). The second part is the spectral mixture analysis using endmembers collected in Georgia (Section 3.3). The third part is monitoring forest degradation using CCDC-SMA, which combines the spectral mixture analysis and the CCDC algorithm on the Google Earth Engine (Section 3.4). Fig. 2 shows the CCDC-SMA workflow. The fourth part is accuracy assessment and area estimation (Section 3.5). We followed the "good practices" in Olofsson et al. (2014) for unbiased area estimation of forest degradation, deforestation, forest, and non-forests in the country of Georgia.

### 3.2. Land cover classification

Classification of land cover is needed before monitoring forest degradation and deforestation. In total, 2695 training points of eight land cover classes in 2000 across our study area were collected: 960 for deciduous forests, 175 for coniferous forests, 131 for mixed forests, 465 for farmland, 503 for shrub or grass, 182 for water or wetland, 110 for barren, and 169 for human settlement (Fig. 3(a)). The training points were collected in areas with stable land cover to enable identification of the land cover using time series of Landsat data and high-resolution imagery with high confidence.

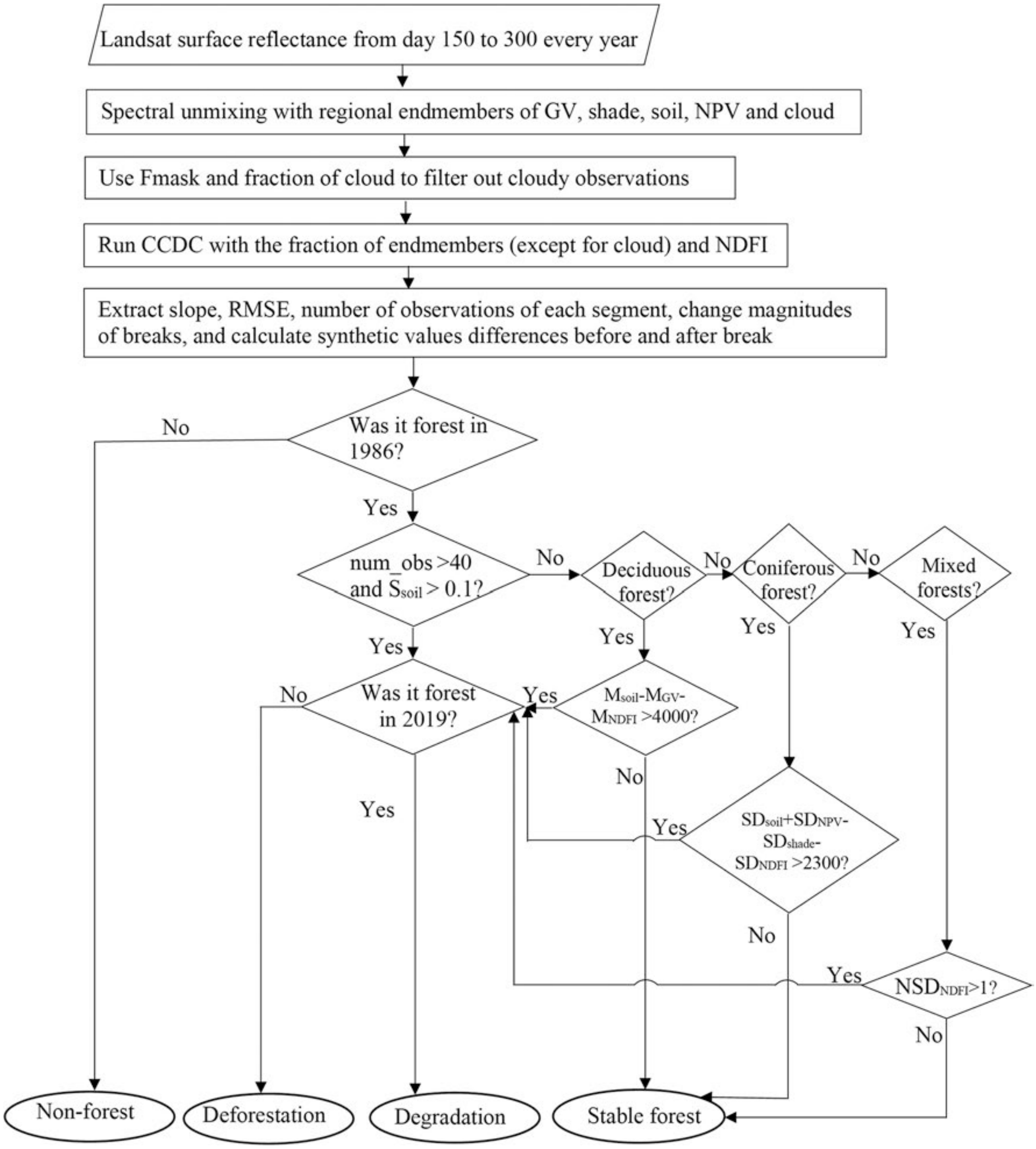


**Fig. 2.** Workflow of CCDC-SMA. The reflectance and fractions are scaled up by 10,000. (num_obs: number of observations; $S_{soil}$: slope of fraction of soil; $M_{soil}$, $M_{GV}$, $M_{NDFI}$: change magnitude (observed values minus predicted values) of fraction of soil, fraction of green vegetation (GV), and Normalized Difference Fraction Index (NDFI), respectively; $SD_{soil}$, $SD_{NPV}$, $SD_{shade}$ and $SD_{NDFI}$: Synthetic value Differences: Synthetic value (the predicted values on July 31st based on the model) of fraction of soil, fraction of non-photosynthetic vegetation (NPV), fraction of shade and NDFI after break minus those before break, respectively; $NSD_{NDFI}$: Normalized Synthetic value Differences: Synthetic value of NDFI before break minus that after break, normalized by the Root Mean Square Error (RMSE) of the segment before the break.) (For interpretation of the references to colour in this figure legend, the reader is referred to the web version of this article.)

We used the CCDC function on GEE to classify annual land cover from 1986 to 2019. The CCDC algorithm uses harmonic models to predict the surface reflectance for any given date. A "break" is triggered if the predicted reflectance significantly deviates from the observed reflectance for a certain number (six in this study) of consecutive observations. After a break, a new model (temporal segment) is initiated. This process is repeated for the whole time series (Zhu and Woodcock, 2014b). We used the full CCDC model that uses 8 coefficients to model reflectance for each band, as explained in Zhu et al. (2015). The harmonic regression model used by CCDC is shown in Eq. (1):

$$p(i,t) = a_{0,i} + s_i t + a_{1,i}.cos\left(\frac{2\pi}{T}t\right) + b_{1,i}.sin\left(\frac{2\pi}{T}t\right) + a_{2,i}.cos\left(\frac{4\pi}{T}t\right) + b_{2,i}.sin\left(\frac{4\pi}{T}t\right) + a_{3,i}.cos\left(\frac{6\pi}{T}t\right) + b_{3,i}.sin\left(\frac{6\pi}{T}t\right) \quad (1)$$

where,

*p(i, t)*: the predicted value of *i*th Landsat Band on Julian date *t*.
*t*: Julian date.
*i*: the *i*th Landsat Band.
*T*: number of days per year ($T = 365.25$).

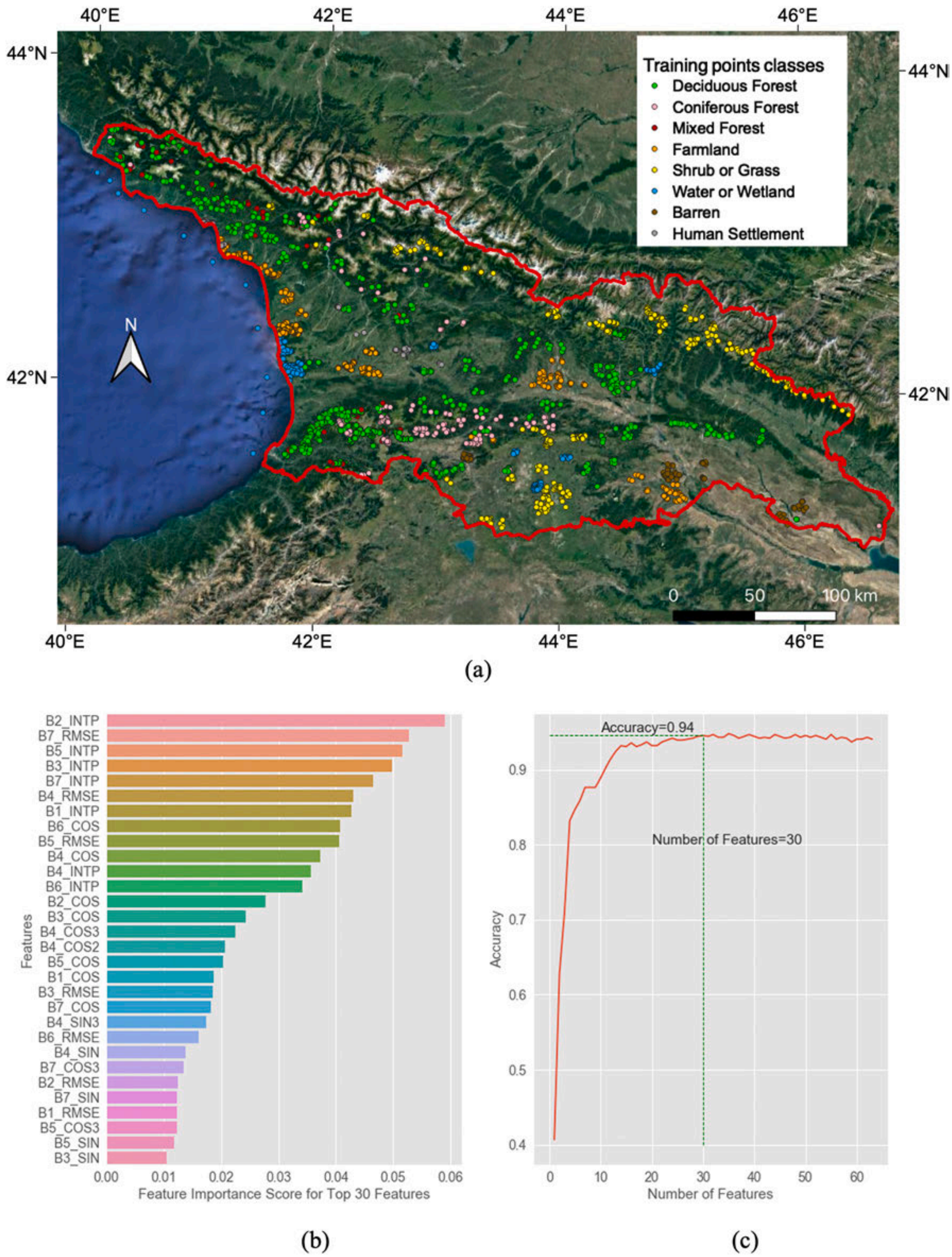


**Fig. 3.** Training data and feature selection for land cover classification: (a) Training data; (b) Feature importance score for the most important 30 features (The feature name consists of the spectral bands and coefficient names. For example, "B2_INTP" stands for the intercept of the green band. B1–B7 stands for blue, green, red, NIR, SWIR1, thermal and SWIR2 band.); (c) Overall accuracy versus number of features. (For interpretation of the references to colour in this figure legend, the reader is referred to the web version of this article.)

$a_{0,i}$: intercept value for the $i$th Landsat band (INTP in Fig. 3(b)).

$s_i$: coefficient for inter-annual change (slope) for the $i$th Landsat band.

$a_{1,i}$, $b_{1,i}$: coefficients for intra-annual change for the $i$th Landsat band (COS and SIN in Fig. 3(b)).

$a_{2,i}$, $b_{2,i}$: coefficients for intra-annual bimodal change for the $i$th Landsat band (COS2 and SIN2 in Fig. 3(b), respectively).

$a_{3,i}$, $b_{3,i}$: coefficients for intra-annual trimodal change for the $i$th Landsat Band (COS3 and SIN3 in Fig. 3(b), respectively).

The original bands (blue, green, red, NIR(Near Infrared), SWIR1 (Short-wave Infrared 1), SWIR2(Short-wave Infrared 2), and thermal band) in all available Landsat data were used to run the CCDC algorithm

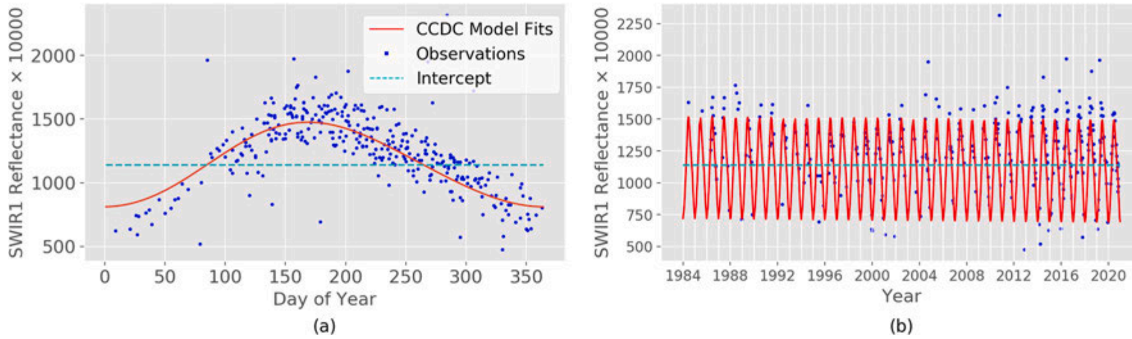


**Fig. 4.** Day of year plot (a) and time series plot (b) of Landsat observations and CCDC model fits of a stable forest pixel.

on GEE from 1984 to 2019. The Tmask algorithm using the green and SWIR1 bands was used to mask cloud pixels (Zhu and Woodcock, 2014a). Spectral-temporal features, such as the intercept, slope, and harmonic regression coefficients were calculated for each spectral band. Fig. 4 shows the spectral-temporal signature and time series of the CCDC model fits and observations of a stable forest pixel. Spectral-temporal features of the segments that intersect with the year 2000 were used to select the 30 most important features for classification (Fig. 3(b)). To test the performance of the top 30 features, we split the training data into two subsets: 70% of data for training and the remaining 30% data for testing. The relationship between the number of features in the classification and the overall accuracy of the test data is shown in Fig. 3 (c). The 30 most important features were used in our final classification, since the overall accuracy of the test classification did not increase when using more than 30 features.

Each time segment was classified to produce annual land cover maps from 1986 to 2019 (the maps of 1984 and 1985 were not used due to limited data for the initial model). After the initial classification, barren and human settlement were merged which resulted in annual land cover maps of seven classes: deciduous forests, coniferous forests, mixed forests, farmland, shrub or grass, water or wetland, and non-vegetated. Fig. 5 shows the land cover map of 2019. Furthermore, the land cover maps were merged into forest and non-forest classes for monitoring forest degradation and deforestation.

### 3.3. Spectral mixture analysis

Five endmembers were collected in our study area: green vegetation (GV), non-photosynthetic vegetation (NPV), soil, shade, and cloud. Candidate endmembers were selected in Landsat imagery and high-resolution imagery acquired close in time (primarily Airbus imagery with a spatial resolution of 0.5 m on Google Earth). In total, we selected 52 candidate pixels for GV endmembers in pure herbaceous regions with almost 100% green leaf cover, 10 candidate pixels for NPV endmembers in regions covered by dry leaves in October, 50 candidate pixels for soil endmembers in pure soil areas, and 50 candidate pixels for cloud endmembers in pure cloud pixels across different landscapes in Georgia. The reflectance of final endmembers was calculated as the mean of the reflectance of candidate endmembers (Fig. 6 and Table 1). The endmember of shade was assigned to zero reflectance at all wavelengths (photometric shade).

We used a linear spectral mixture analysis model to calculate the fraction of endmembers and constrained the fractions to be non-negative and sum to one. To evaluate the SMA model, we created composites of

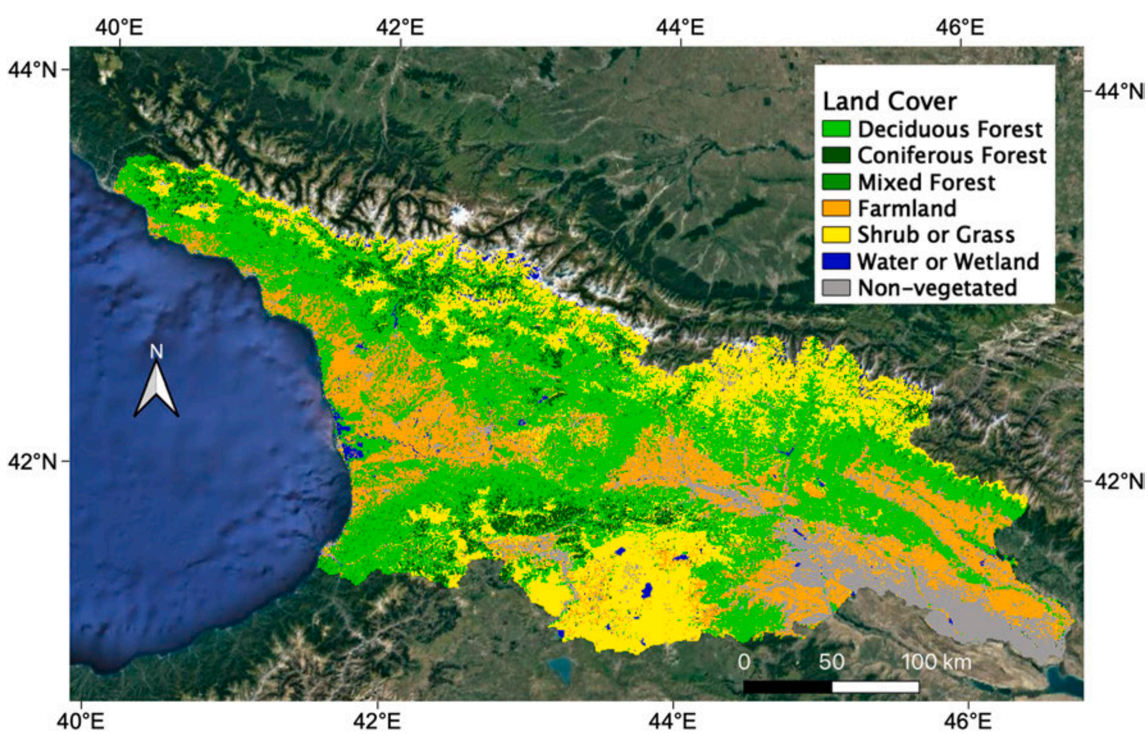


**Fig. 5.** Land cover map of Georgia in 2019.

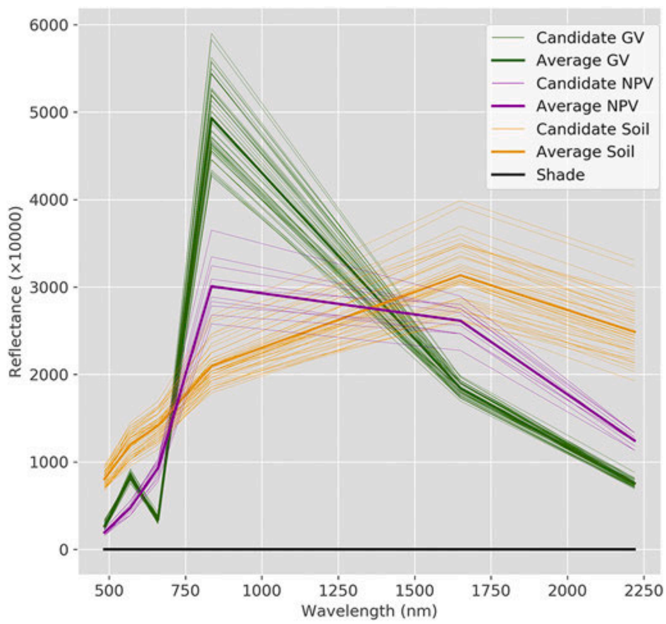


**Fig. 6.** Spectral profile of the GV, NPV, soil, and shade endmembers collected in Georgia.

**Table 1**
Landsat surface reflectance × 10,000 of the GV, NPV, soil, shade, and cloud endmembers collected in Georgia.

| | Original bands | | | | | |
|---|---|---|---|---|---|---|
| Endmembers | Blue | Green | Red | NIR | SWIR 1 | SWIR 2 |
| GV | 264 | 832 | 338 | 4931 | 1841 | 754 |
| Soil | 803 | 1199 | 1414 | 2094 | 3134 | 2487 |
| NPV | 192 | 476 | 929 | 3007 | 2613 | 1243 |
| Shade | 0 | 0 | 0 | 0 | 0 | 0 |
| Cloud | 1678 | 1986 | 1884 | 4518 | 3404 | 2148 |

the country of Georgia using the median reflectance from May to August in six selected years and calculated the RMSEs of the SMA model, respectively. The average RMSEs of the whole country in the six selected years, 1990, 1995, 2000, 2005, 2010, and 2018, were 81, 83, 75, 79, 75, and 84 (the reflectance is scaled up by 10,000), respectively, which are all very low. Fig. 7 shows the RMSE of the SMA model for the composite in 2018 as an example.

Normalized Difference Fraction Index (NDFI), developed by Souza et al. (2005), was calculated using Eq. (2) (a mask of fraction of shade to be less than 1 was applied, so that Eqs. (2) and (3) can be correctly calculated):

$$NDFI = \frac{GV_{shade} - (NPV + Soil)}{GV_{shade} + (NPV + Soil)} \quad (2)$$

where,

$$GV_{shade} = \frac{GV}{1 - shade} \quad (3)$$

NDFI has been successfully used by Souza et al. (2005) and Bullock et al. (2020a) to monitor forest degradation in the tropics but has not been used in temperate regions. Fig. 8 shows an example of spectral unmixing in our study area. In general, grassland, farmland, and dense deciduous forests during the growing season have high fractions of GV, low fractions of soil and NPV. Coniferous forests have high fractions of shade and lower fractions of GV compared with deciduous forests. Dense deciduous forests and coniferous forests both have high values of NDFI. NDFI and the fraction of GV, soil, shade, and NPV were used to run CCDC-SMA. The fraction of cloud and Fmask (Zhu and Woodcock, 2012) were used to filter out cloudy observations.

### 3.4. Forest degradation monitoring

There are two types of forest degradation in Georgia: abrupt and gradual, both of which affect deciduous, coniferous, and mixed forests. Abrupt degradation results in “breaks” in the time series and is caused by events such as harvesting for fuelwood or lumber, sanitary logging, pest damage, drought, and wildfire. Fig. 9 shows an example of an abrupt degradation event in a deciduous forest in Georgia in 2008. From 2000

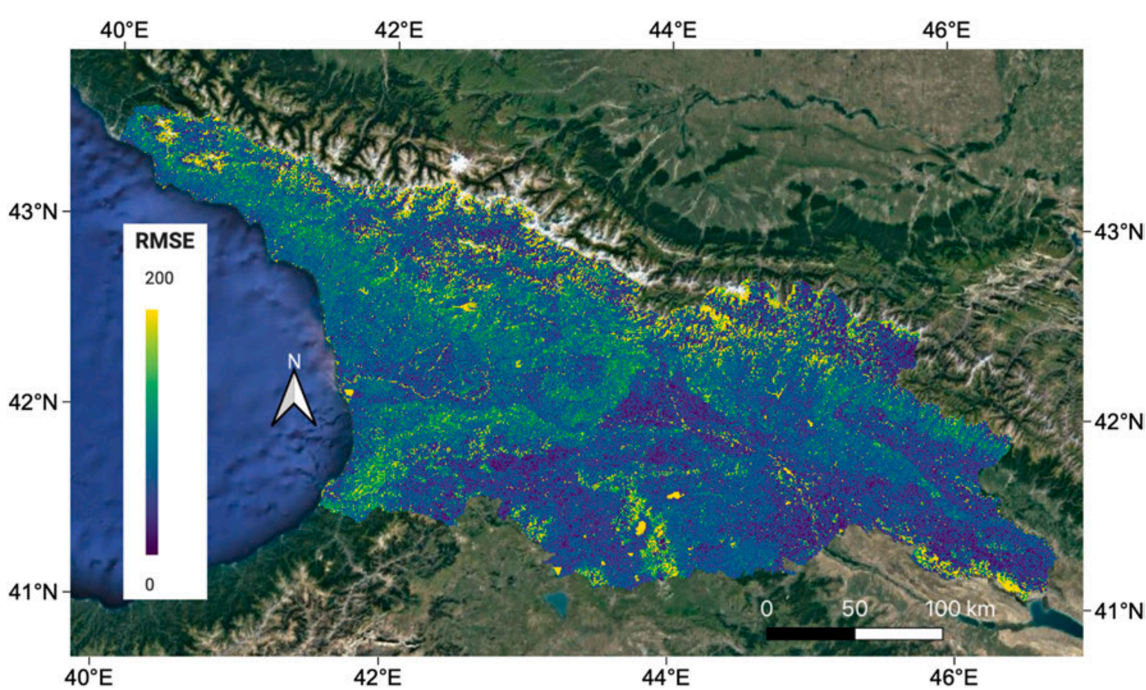


**Fig. 7.** RMSE of the SMA model of a summer composite in 2018. (The reflectance is scaled up by 10,000.)

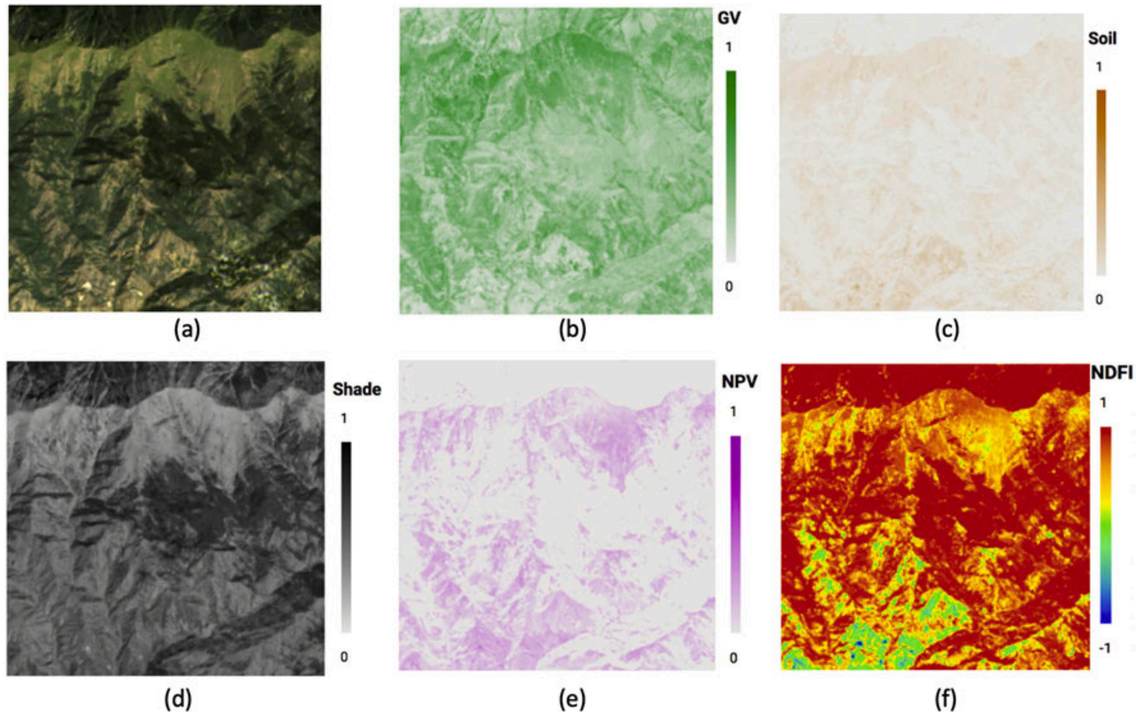


**Fig. 8.** An example of spectral unmixing of a Landsat image: (a) Landsat image (red-green-blue); (b) fraction of GV; (c) fraction of soil; (d) fraction of shade; (e) fraction of NPV; (f) NDFI. (For interpretation of the references to colour in this figure legend, the reader is referred to the web version of this article.)

to 2008, the fraction of soil was close to zero, since the pixel was located in a dense forest with almost no exposure of soil, which is evident by the high-resolution image in 2003. In 2008, a logging event and construction of roads led to an opening of the tree canopy and exposure of soil, which triggered an abrupt decrease in NDFI and fraction of GV, as well as an abrupt increase in the fraction of soil and NPV. After the disturbance in 2008, the forest started recovering, causing a gradual increase in the fraction of GV and NDFI, and a gradual decrease in the fraction of soil and NPV. The recovery of trees is evident in high-resolution imagery in 2013 and 2018. In contrast, gradual degradation is represented as

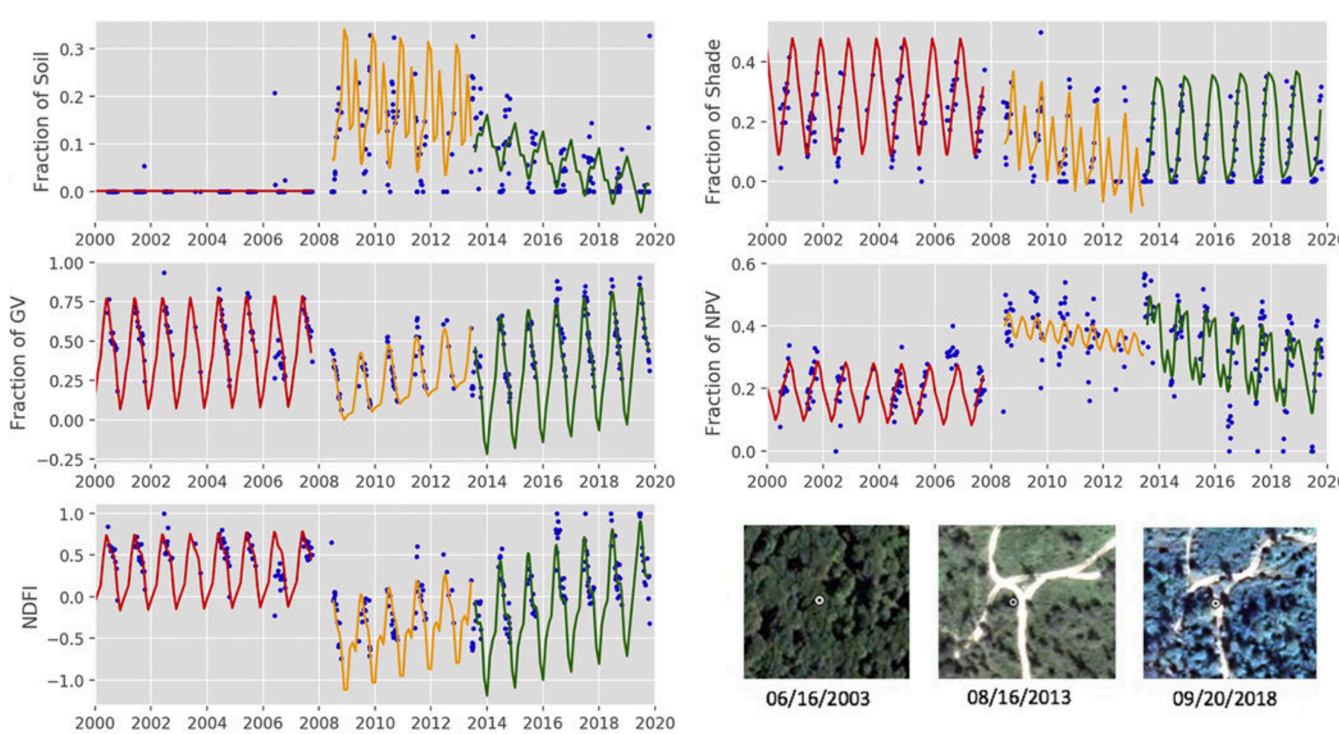


**Fig. 9.** Time series of a pixel that experienced an abrupt degradation event in 2008 (location: 42° 6′1.14″N, 43°34′3.70″E). The blue points show the Landsat observations from day 150 to 300 every year. The lines with different colors show different segments of CCDC-SMA model fits. The white circles in high-resolution images show the center of the pixel. (For interpretation of the references to colour in this figure legend, the reader is referred to the web version of this article.)

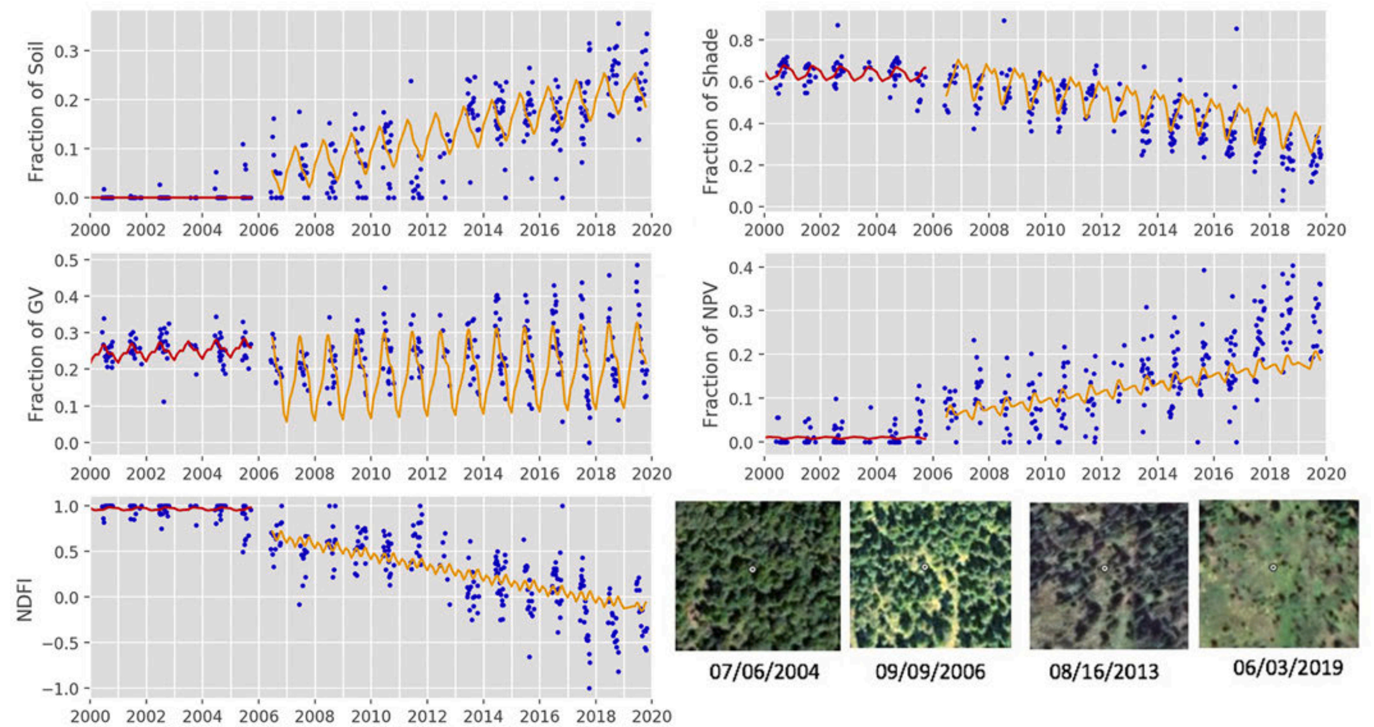


**Fig. 10.** Time series of a pixel that experienced a gradual forest degradation process from 2006 to 2019 (location: 41°47′4.80″N, 43°28′33.99″E). The blue points show the Landsat observations from day 150 to 300 every year. The lines with different colors show different segments of CCDC-SMA model fits. The white circles in high-resolution images show the center of the pixel. (For interpretation of the references to colour in this figure legend, the reader is referred to the web version of this article.)

"segments" with slopes rather than breaks in the time series and is caused by a series of degradation events, such as continuous extraction of individual trees (often a result of illegal logging). Fig. 10 shows an example of gradual degradation in a coniferous forest that started in 2006 and continued until 2019. Before 2006, the fraction of soil was close to zero, since this location was a dense forest that had little soil exposed as shown in high-resolution image in 2004. From 2006 to 2019, the continuous extraction of individual trees led to gradual decrease in NDFI and the fraction of shade, and gradual increase in the fractions of soil and NPV. The seasonal variations and maximum value of the fraction of GV both increased, indicating a transition from coniferous forests to grass and broadleaved shrubs. The high-resolution imagery in Fig. 10 shows the gradual decrease in tree density from 2006 to 2019.

To explore how the fractions of different endmembers respond to forest degradation, we investigated 113 locations (69 in deciduous forest, 22 in coniferous forest, and 22 in mixed forest) in regions where forest degradation is clearly visible in high-resolution images in Google Earth for at least two different years. Two interpreters examined and recorded how different indices changed (increase, decrease or no-change) and then sorted the sites by forest type and direction of change of indices. Based on this analysis, we found that SMA-based indices are more effective in observing changes compared to the original Landsat bands (red, NIR, and SWIR1) and traditional vegetation indices (NDVI(Normalized Difference Vegetation Index) and EVI (Enhanced Vegetation Index)). Results of this analysis are explained in Section 4.1.

Based on the analysis of the sensitivity of the indices, we used the fraction of endmembers and NDFI as the inputs to the CCDC algorithm as they are more sensitive to forest degradation than the original spectral bands. Unlike the original CCDC algorithm that uses spectral bands and observations from the entire year, we used fractions of endmembers and NDFI from day 150 to day 300. Using observations from part of a year reduced the seasonal variability in the data, which resulted in better model fitting and minimized the risk of the model being affected by snow. The data density during the 1980s is rather low, and thus only using summer observations is unfavorable.

To find the optimal metrics for monitoring forest degradation, we ran CCDC with the SMA-based indices from 1987 to 2019 at 724 testing locations (390 breaks and 334 segments). We selected locations where the Landsat data density is high, high-resolution imagery is available, and the segments or breaks in the CCDC-SMA model are easy to interpret. The testing locations are distributed at different parts of the country and cover different climatic conditions. Tables 2 and 3 show the number of breaks and segments at testing sites, respectively. Some breaks were triggered by degradation, whereas other breaks were triggered by recovery or noise in the data. Some segments were caused by gradual degradation, whereas other segments represented stable conditions or recovery.

Abrupt degradation is represented as "breaks" in the CCDC-SMA model, but not all breaks are associated with forest disturbance. To find the best metric for detecting abrupt degradation, we investigated the change of SMA-related indices in the presence of abrupt degradation in different forest types, including deciduous, coniferous, and mixed forests. In addition, three different methods of calculating the magnitude of change were investigated (Fig. 11): First, using the observed values minus predicted values (Fig. 11(a)). This method would be the best in cases where the forest recovered quickly after the disturbance, since the characteristics of the segment before and after the break could be quite similar. Second, using synthetic value differences before and after the break (Fig. 11(b)). This method might be the best in cases where the model fitting was good in the peak growing season, but poor in other times of year. Third, using intercept differences before and after the break (Fig. 11(c)). This method could be the best if the degradation event changed the spectral characteristic of the segment (e.g., intercept) but did not substantially change the values in the peak growing season. We also tested if normalizing the magnitude by the RMSE of the segment

**Table 2**
Number of test breaks.

| Forest type | Type of break | Number of test breaks |
|---|---|---|
| Coniferous forest | Degradation | 91 |
| Coniferous forest | No degradation | 92 |
| Deciduous forest | Degradation | 78 |
| Deciduous forest | No degradation | 75 |
| Mixed forest | Degradation | 22 |
| Mixed forest | No degradation | 32 |
| Total | All | 390 |

**Table 3**
Number of test segments.

| Forest type | Type of segment | Number of test segments |
|---|---|---|
| Coniferous forest | Degradation | 100 |
| Coniferous forest | No degradation | 100 |
| Deciduous forest | Degradation | 51 |
| Deciduous forest | No degradation | 51 |
| Mixed forest | Degradation | 16 |
| Mixed forest | No degradation | 16 |
| Total | All | 334 |

before the break increased accuracy.

Overall accuracy was calculated using a total of 102 combinations of indices, methods of calculating change magnitude and normalization to find an optimal threshold for abrupt degradation (Fig. 12). We found that the optimal metric for deciduous forest degradation was using the observed minus predicted values of (soil-GV-NDFI), whereas the optimal metric for coniferous forest degradation was the difference between synthetic values of (soil+NPV-Shade-NDFI) before and after the break (Fig. 13). For mixed forest, the optimal metric was the synthetic value differences of NDFI before and after the break, normalized by RMSE of the segment before the break. If combining all types of forest, the optimal metric is the magnitude (observed minus predicted) of (soil-NDFI). However, the overall accuracy would be lower if combining all types of forests, compared with using different optimal indices for different types of forest. If combining all types of forest and only using a single index alone, the optimal metric was using the magnitude (observed minus predicted) of NDFI.

While the results above suggest that using different metrics for different forest types is better than using a single metric for all types of forests, we wanted to verify the finding by calculating accuracies from a random sample with 500 units drawn from the area where these two maps differed: one using a single metric (soil- NDFI) and the other one using different metrics for different forest types. Each sample unit was labelled as disturbed or undisturbed after examination of reference data, and overall accuracy was calculated. The sampling-based approach verified the finding that using different metrics for different forest types was more accurate than using a single metric for all types of forests (10% higher).

Similar tests were done to determine the optimal metric to monitor gradual degradation (Fig. 14). A total of 17 combinations of types of forests and slope of indices were tested. We found that, as opposed to abrupt degradation, using different metrics for different forest types did not result in higher accuracy. Instead, the slope of the soil fraction was found to be the best for monitoring gradual degradation in all forest types (Fig. 15).

After these tests, we developed a final workflow for CCDC-SMA, shown as Fig. 2. A suite of Google Earth Engine Apps and codes to run CCDC-SMA, visualize the time series of CCDC-SMA model fits and display the map products of this study is hosted on https://github.com/shijuanchen/forest_degradation_georgia.

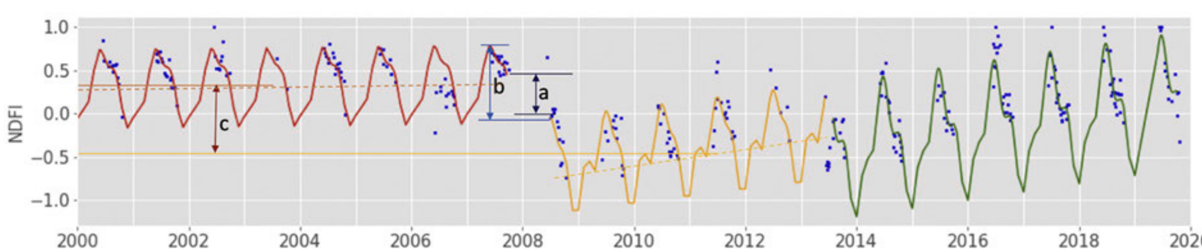


**Fig. 11.** Different ways of calculating the magnitude of change: (a) The median of the observed minus predicted values for the next 6 consecutive observations after the break (CCDC default). (b) Differences between the predicted values on July 31st (called synthetic values) before and after the break. July 31st was chosen since the predicted values in the peak growing season are more accurate than those in other seasons. (c) Differences between the intercepts at the midpoint of segments before and after the break.

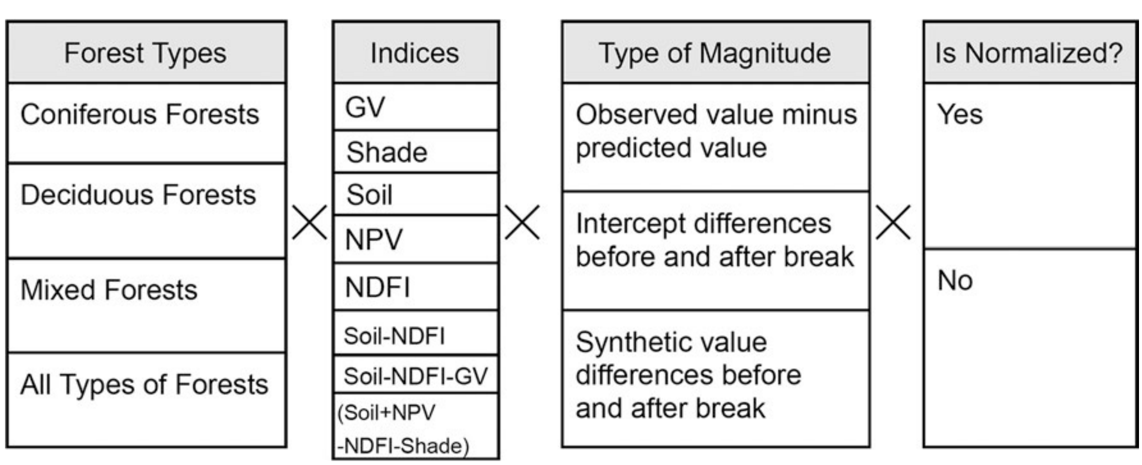


**Fig. 12.** Testing different combinations to find the optimal indices and thresholds for monitoring abrupt degradation.

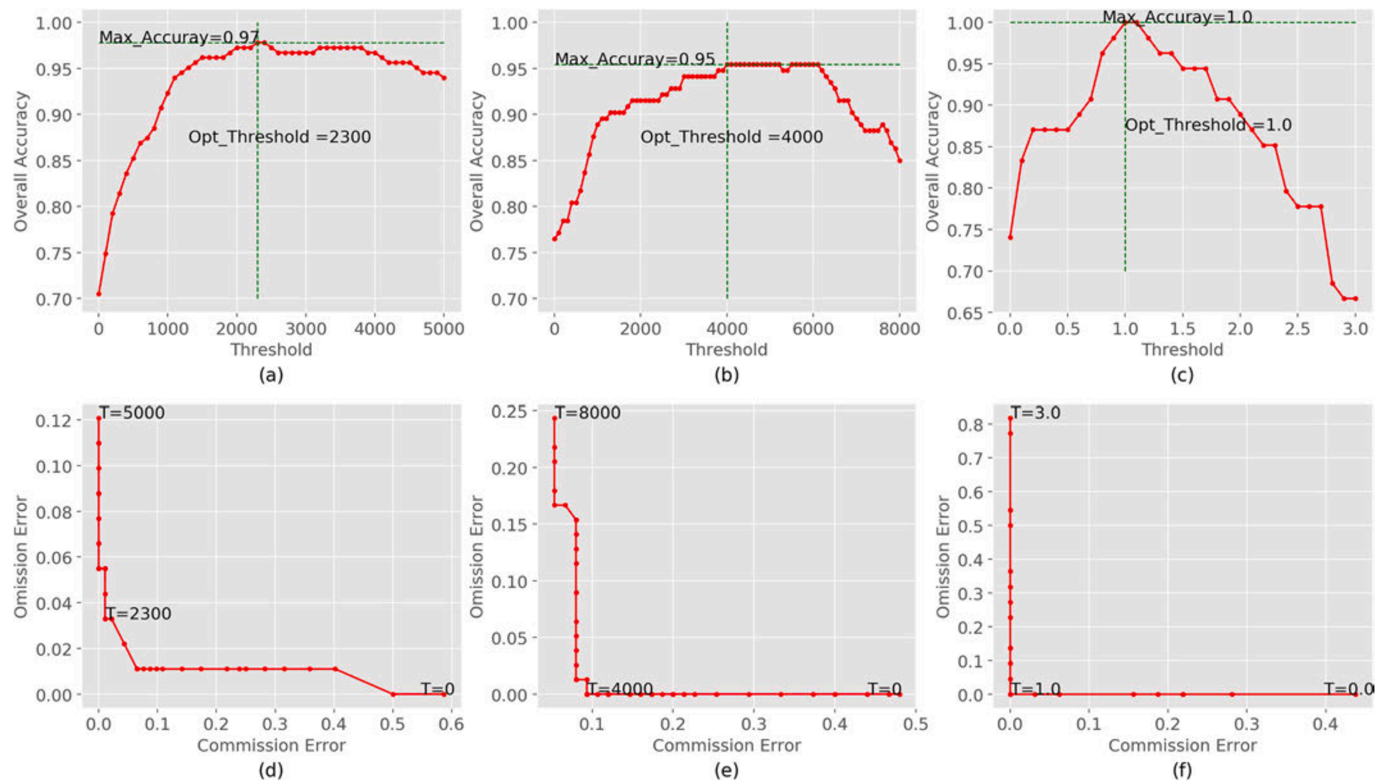


**Fig. 13.** Testing results of abrupt degradation (Max_Accuracy: highest accuracy; Opt_Threshold: optimal threshold; T: threshold): Overall accuracy versus threshold for test samples in (a) coniferous forests, (b) deciduous forests, and (c) mixed forests; Omission and commission errors using different thresholds in (d) coniferous forests, (e) deciduous forests, and (f) mixed forests.

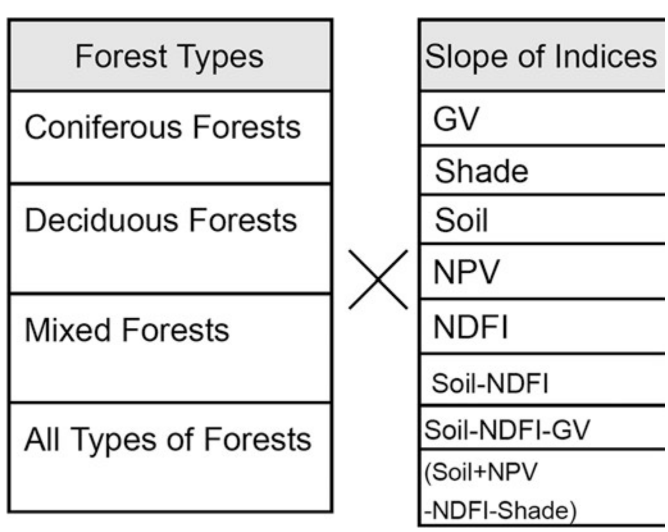


**Fig. 14.** Testing different combinations to find the optimal indices and thresholds for monitoring gradual degradation.

To further improve our results, we implemented two post-processing steps based on spatial information. The first step was to remove isolated pixels mapped as disturbed from the final degradation map as such pixels were often misclassified. The second step was to minimize omission errors by adding pixels, where a break was triggered by CCDC-SMA model and a majority of pixels in a 3 × 3 pixel window surrounding it had been mapped as disturbance, to the final degradation map, even if those pixels may be mapped as undisturbed originally.

Although our major goal was to monitor forest degradation, characterizing the post-disturbance status of the land surface is useful in subsequent analyses of the carbon emissions and policy implications. We tried to determine whether the forest experienced recovery at the end or not by examining the slope of the model fit. A pixel would be mapped as recovery if the time series segments at the end exhibited a positive slope of NDFI or a negative slope of fraction of soil.

### 3.5. Accuracy assessment and area estimation

Following recommended practices in the literature (Olofsson et al., 2014), areas of forest degradation and deforestation and the accuracy of the maps over our study period from 1987 to 2019 were estimated by sampling. The population to be sampled was all the 30 m × 30 m Landsat pixels covering the study area. A sample was drawn from this population under stratified random sampling to ensure sufficient statistical representation in areas with deforestation and degradation. Strata were created to corresponding classes of which we intended to estimate areas and assess accuracies:

- *Stable forest (st_forest):* stable forest without disturbance in our study period.
- *Non-forest (non_forest)*: non-forest area, including shrub, grassland, farmland, non-vegetated, water, and wetland.
- *Deforestation (defor)*: Conversion from forest to non-forest.
- *Degradation with recovery (deg_re)*: forest experienced degradation in our study period, with recovery signal at the end.
- *Degradation without recovery (deg_no_re)*: forest experienced degradation in our study period, without recovery signal at the end.

In addition, two strata were created to mitigate the anticipated impact of omissions of degradation and deforestation. Omission errors of small classes (such as deforestation and degradation) that occur in large strata (typically stable forest) have been reported and shown to introduce considerable uncertainty in final area estimates (Olofsson et al.,

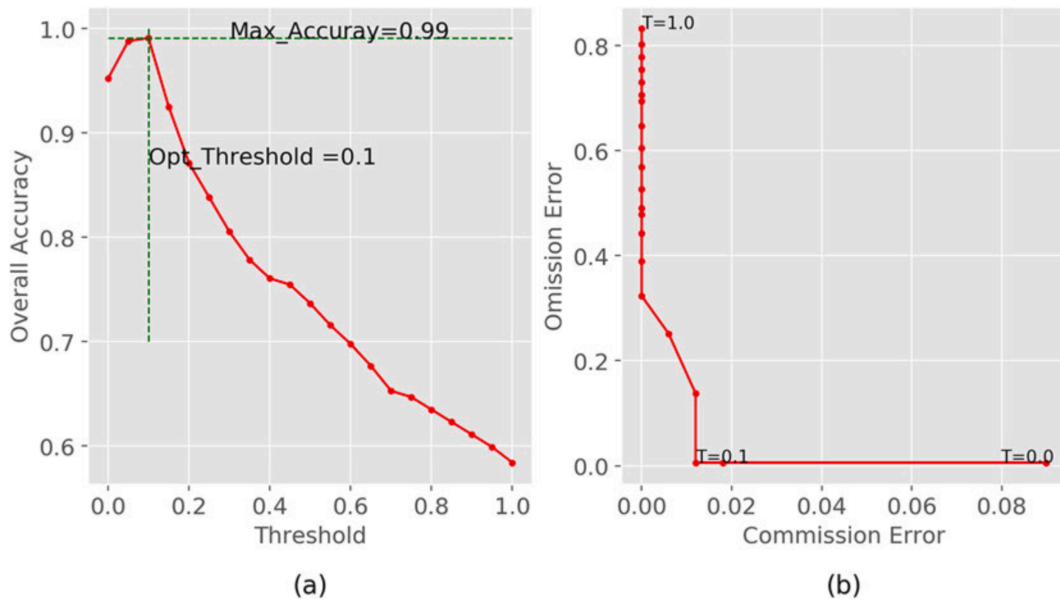


**Fig. 15.** Testing results of gradual degradation (Max_Accuracy: highest accuracy; Opt_Threshold: optimal threshold; T: threshold): (a) Overall accuracy versus threshold; (b) Omission and commission errors using different thresholds.

2020). The impacts of such omission errors are mitigated if the large stratum is split into a substratum where omission errors are less likely to occur and a much smaller substratum where omission errors are more likely to occur. For this reason, we created two additional strata, *deforestation buffer* and *possible degradation*:

- *Deforestation buffer (defor_buffer)*: 1-pixel buffer around the deforestation stratum to mitigate omission errors of deforestation.
- *Possible degradation (pos_deg)*: designed to mitigate omissions of forest degradation; pixels that meet one of the conditions were included: (1) isolated pixels before post processing; (2) pixels mapped as disturbed in a previous version of the map (Section 3.4 the map using (soil-NDFI)) but not in the final version; (3) pixels adjacent to at least two disturbed pixels in a 3 by 3 window; (4) pixels adjacent to at least one pixel with a negative NDFI slope in a 3 by 3 window.

We determined the sample size by setting a target precision corresponding to a 15% margin of error (defined as two times the standard error divided by the area estimate) of the area of forest degradation. Cochran (1977, eq. 5.25) suggests solving the stratified variance estimator to calculate the sample size required to reach a target variance (or preferably a standard error or confidence interval). The stratified variance estimator suggested a sample size of 1105 to achieve a margin of error of 15%. For estimation of area, an optimal allocation is very close to an allocation proportional to the size of the strata but with a minimum sample size of 30 units per stratum (Olofsson et al., 2020). Following this rationale, we allocated the sample to strata as shown in Table 4.

Two interpreters determined reference conditions at each sample unit location by careful examination of reference data from 1987 to 2019 consisting of Landsat time series and high-resolution images in Google Earth using AREA2 (Arévalo et al., 2020). An example of a sample unit that experienced forest degradation is provided in Fig. 16. The reference data available in this case are two high-resolution images in 2007 and 2019 and Landsat time series of fraction of soil, GV, shade, NPV, and NDFI from 1984 onwards. In the time series plots, an abrupt increase in fraction of soil and NPV and an abrupt decrease in fraction of GV and NDFI in 2017 indicated a logging event in 2017, which is also evident by comparing the Landsat images and the high-resolution images before and after the change (Fig. 16). The interpreters also recorded the level of confidence (high, middle, or low) in their reference labels. Sample units with observations with middle or low confidence were examined and discussed in a team effort with local land cover experts. After interpretation and discussion, 25 sample units were discarded due to a lack of reference data, which resulted in a final sample size of 1080 units. This may introduce a very small bias, but the effect would be minimal and removing them is better than guessing since no reference data is available at these locations.

Following interpretation, a stratified estimator was constructed for estimation of map accuracy and area, and confidence intervals were estimated using a stratified variance estimator (Cochran, 1977). The stratified estimator is unbiased and can be regarded as adjusting for the errors of omission and commission in the map. The term estimator is used here in a statistical context and refers to the formula by which estimates of population parameters are calculated from the sample results. The estimator is unbiased, if the bias of an estimator of a population parameter, defined as the difference between the expected value and the true value over all possible samples, is zero (Casella and Berger, 2002).

## 4. Results

### 4.1. Sensitivity of SMA-based indices

Based on the visual interpretation of time series of the 113 locations that we explained in Section 3.4, we found that SMA-based indices are

**Table 4**
Map area, strata weights, and sample allocation.

| Stratum | defor | defor_buffer | deg_re | deg_no_re | pos_deg | st_forest | non_forest | Total |
|---|---|---|---|---|---|---|---|---|
| Map area [km$^2$] | 216 | 653 | 3280 | 954 | 2015 | 24,336 | 38,202 | 69,656 |
| Strata weights | 0.003 | 0.009 | 0.047 | 0.014 | 0.029 | 0.349 | 0.548 | 1.000 |
| Sample allocation | 30 | 30 | 50 | 30 | 50 | 360 | 555 | 1105 |

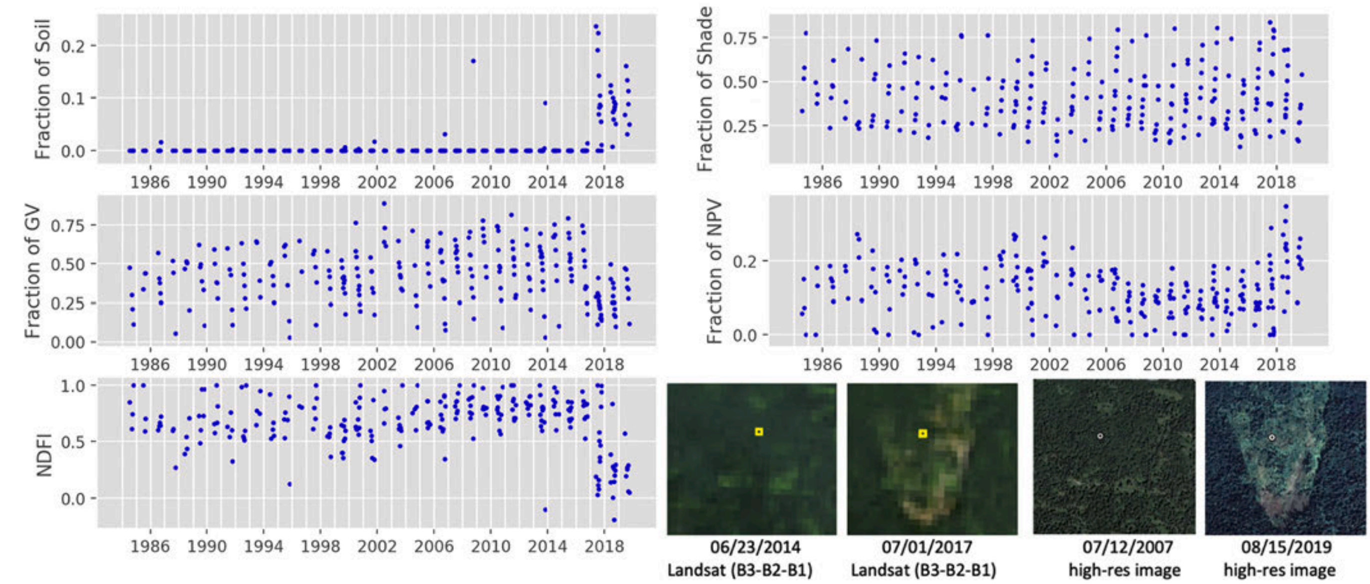


**Fig. 16.** An example of a sample unit that experienced forest degradation in 2017 (location: 43°5′32.86″N, 41°51′49.65″E). Blue points are Landsat observations. (For interpretation of the references to colour in this figure legend, the reader is referred to the web version of this article.)

more effective in observing changes compared to the original Landsat bands (red, NIR and SWIR1) and traditional vegetation indices (NDVI and EVI). Table 5 shows the proportion of sites in each forest type and indices. For example, the cell for row "NDFI" and column "DE" has a value of 0.93, which means that in 93% of the deciduous forest sites a decrease in NDFI was observed. If change of an index was observed for more than 80% of the sites in a certain forest type, we considered that the index is sensitive to degradation in this forest type. We found that the best single index is NDFI followed by fraction of soil, both of which are effective for all forest types.

Furthermore, we found that fraction of shade and fraction of GV have difference sensitivity in coniferous forest and deciduous forest. Fraction of shade is effective for observing coniferous forest degradation but not so for deciduous forest degradation. Dense coniferous forests are associated with high fractions of shade. When degradation occurs, more soil and understory are exposed, which lead to increase of pixel brightness and decrease of fraction of shade. Dense deciduous forests, however, are associated with low fractions of shade. Extraction of individual deciduous trees may cause canopy gaps and more exposure of shadows of surrounding tree crowns, which leads to higher fraction of shade. In other cases, when the gaps are large enough to expose soil and understory vegetation, fraction of shade tends to decrease. Moreover, we found that fraction of GV is effective for observing deciduous forest degradation, as more soil or dry vegetation (e.g., stumps) on the forest floor results in a decrease in fraction of GV. This is usually not the case with dense coniferous forests which are associated with low fractions of GV. Harvesting coniferous forest usually leads to an increase in fraction of GV, since more understory vegetation associated with higher fraction of GV is exposed after degradation. In the event of fire or pest damage, however, fractions of GV often decrease, even in coniferous forests. Note that this analysis of change of indices did not include any model fitting or algorithm tuning, and thus is not affected by bad model fitting or errors in a change detection algorithm.

Moreover, we investigated the sensitivities of SMA-related indices with CCDC-SMA model fitting in different types of forest. As we mentioned in Section 3.4, we ran CCDC-SMA from 1987 to 2019 at 724 testing locations (390 breaks and 334 segments). Fig. 17 shows the distribution of slopes and change magnitudes of the fraction of GV, shade, and NPV in different types of forests. The "slopes" here refers to the slopes of the segments of CCDC-SMA models. The change magnitudes are the observed values minus predicted values when CCDC-SMA detects a break. Deciduous forest degradation resulted in a large decrease in fraction of GV (blue region in Fig. 17(a) and (d)) and either an increase or decrease in the fraction of shade (blue region in Fig. 17(b) and (e)); the fraction of NPV tended to increase with abrupt events but gradual deciduous forest degradation sometimes resulted in a decrease (blue region in Fig. 17(c) and (f)). Coniferous forest degradation resulted in either an increase or decrease in fraction of GV (red region in Fig. 17 (a) and (d)), a decrease in the fractions of shade (red region in Fig. 17(b) and (e)), and increase in the fraction of NPV (red region in Fig. 17(c) and

**Table 5**
Proportion of sites in each forest type and indices.

| Forest type | Deciduous forest | | | Coniferous forest | | | Mixed forest | | |
|---|---|---|---|---|---|---|---|---|---|
| Indices | IN | DE | NO | IN | DE | NO | IN | DE | NO |
| NDFI | 0.00 | **0.93** | 0.07 | 0.00 | **1.00** | 0.00 | 0.00 | **0.96** | 0.05 |
| Shade | 0.10 | 0.22 | 0.68 | 0.00 | **0.86** | 0.14 | 0.00 | **0.82** | 0.18 |
| GV | 0.03 | **0.91** | 0.06 | 0.55 | 0.23 | 0.23 | 0.23 | 0.55 | 0.23 |
| NPV | 0.65 | 0.10 | 0.25 | **0.96** | 0.00 | 0.05 | **0.91** | 0.00 | 0.09 |
| Soil | **0.83** | 0.00 | 0.17 | **0.91** | 0.00 | 0.09 | **0.86** | 0.00 | 0.14 |
| SWIR1 | 0.30 | 0.03 | 0.67 | **0.91** | 0.00 | 0.09 | 0.73 | 0.00 | 0.27 |
| NIR | 0.01 | 0.62 | 0.36 | 0.68 | 0.00 | 0.32 | 0.41 | 0.00 | 0.59 |
| NDVI | 0.00 | 0.45 | 0.55 | 0.05 | 0.09 | 0.86 | 0.00 | 0.18 | 0.82 |
| EVI | 0.01 | 0.71 | 0.28 | 0.41 | 0.09 | 0.50 | 0.27 | 0.14 | 0.59 |
| RED | 0.33 | 0.00 | 0.67 | 0.46 | 0.00 | 0.55 | 0.18 | 0.00 | 0.82 |

Proportions larger than 0.8 under increase or decrease columns are highlighted in bold (IN: increase; DE: decrease; NO: no-change).

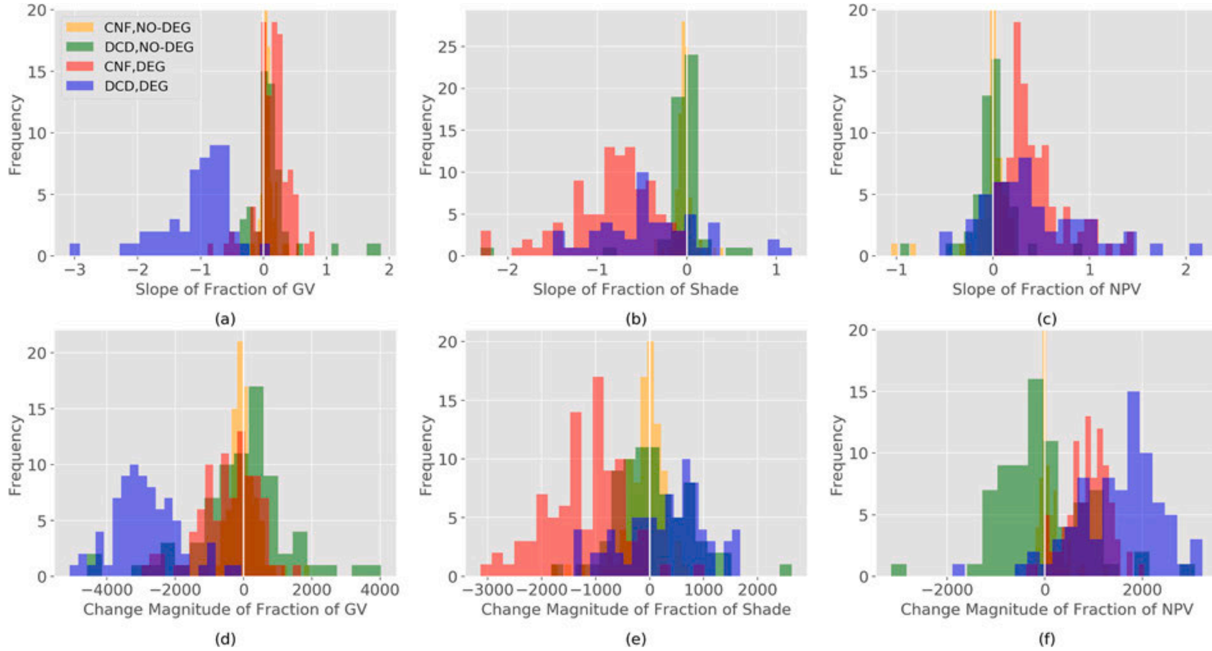


**Fig. 17.** Slopes and change magnitudes of fraction of GV, shade, and NPV in different types of forests (CNF: coniferous forests; DCD: deciduous forests; NO-DEG: no degradation; DEG: degradation).

(f)). In summary, the results suggested that the fraction of GV and shade have different sensitivities in deciduous and coniferous forest degradation, which is consistent with the finding in the visual interpretation. Both the visual interpretation and CCDC-SMA model fitting results suggested that fraction of GV is sensitive to deciduous forest degradation whereas fraction of shade is sensitive to coniferous forest degradation, and that NDFI and fraction of soil are both sensitive to deciduous and coniferous forest degradation.

### 4.2. Accuracies and area estimates

The overall accuracy of our map with the original classes was 89%. Unsurprisingly, both the stable forest and non-forest were mapped with high accuracies, whereas the change classes have relatively lower accuracies (Tables 6 and 7). While the accuracy of the deforestation class might seem low, the area of deforestation was only 0.3% of the study area; mapping and estimating such a small area was inherently difficult.

**Table 6**
Confusion matrix expressed in sample counts, map area and area weights of original classes.

| Reference class | | | | | | | | |
|---|---|---|---|---|---|---|---|---|
| Map strata | defor | deg_re | deg_no_re | st_forest | non_forest | Total | Map area (km$^2$) | Area weight |
| defor | 15 | 1 | 2 | 2 | 9 | 29 | 216.13 | 0.003 |
| defor_buffer | 0 | 4 | 4 | 5 | 17 | 30 | 652.97 | 0.009 |
| deg_re | 0 | 17 | 15 | 13 | 1 | 46 | 3280.00 | 0.047 |
| deg_no_re | 0 | 1 | 18 | 7 | 2 | 28 | 954.49 | 0.014 |
| pos_deg | 1 | 0 | 3 | 38 | 2 | 44 | 2014.80 | 0.029 |
| st_forest | 0 | 1 | 3 | 335 | 11 | 350 | 24,335.61 | 0.349 |
| non_forest | 0 | 0 | 0 | 22 | 531 | 553 | 38,202.02 | 0.548 |
| Total | 16 | 24 | 45 | 422 | 573 | 1080 | 69,656.02 | 1.000 |

**Table 7**
Confusion matrix of original classes expressed in proportions, accuracies, unbiased area estimates and uncertainty of area estimates (area std. error: standard error of area estimates (km$^2$)).

| Reference class | | | | | | | | |
|---|---|---|---|---|---|---|---|---|
| Map strata | defor | deg_re | deg_no_re | st_forest | non_forest | Total | User's accuracy | Producer's accuracy |
| defor | 0.002 | 0.000 | 0.000 | 0.000 | 0.001 | 0.003 | 0.517 | 0.709 |
| defor_buffer | 0.000 | 0.001 | 0.001 | 0.002 | 0.005 | 0.009 | | |
| deg_re | 0.000 | 0.017 | 0.015 | 0.013 | 0.001 | 0.047 | 0.37 | 0.860 |
| deg_no_re | 0.000 | 0.000 | 0.009 | 0.003 | 0.001 | 0.014 | 0.643 | 0.288 |
| pos_deg | 0.001 | 0.000 | 0.002 | 0.025 | 0.001 | 0.029 | | |
| st_forest | 0.000 | 0.001 | 0.003 | 0.334 | 0.011 | 0.349 | 0.957 | 0.837 |
| non_forest | 0.000 | 0.000 | 0.000 | 0.022 | 0.527 | 0.548 | 0.96 | 0.962 |
| Total | 0.002 | 0.020 | 0.031 | 0.400 | 0.547 | 1.000 | | |
| Area Estimates (km$^2$) | 157.582 | 1410.309 | 2131.098 | 27,841.814 | 38,115.218 | | Overall accuracy: 0.889 | |
| 1.96 × (area std error) | 98.262 | 493.719 | 562.998 | 957.530 | 803.448 | | | |
| Margin of error | 0.624 | 0.350 | 0.264 | 0.034 | 0.021 | | | |

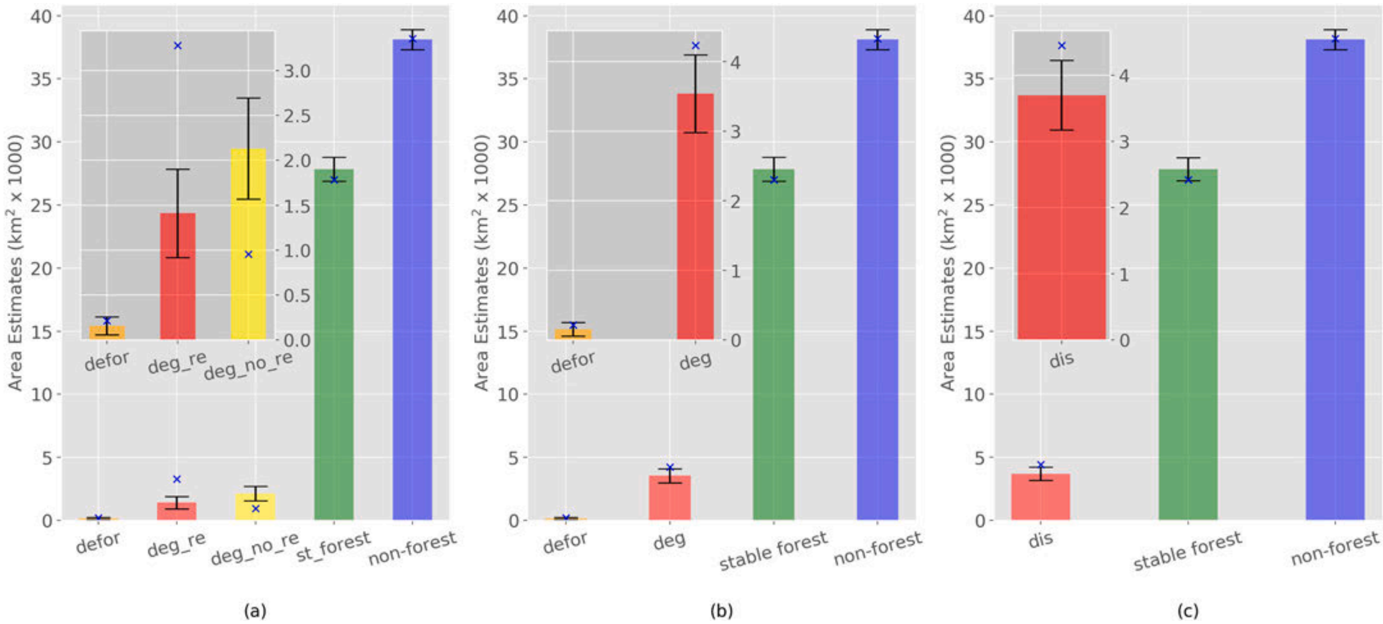


**Fig. 18.** Area estimates with 95% confidence intervals from 1987 to 2019 of (a) deforestation, forest degradation with recovery, forest degradation without recovery, stable forest, and non-forest; (b) deforestation, forest degradation (deg), stable forest, and non-forest; (c) forest disturbance (dis), stable forest, and non-forest. The colored bars show the unbiased area estimates, the black bars show uncertainty, and the blue crosses represent mapped areas based on pixel counting. The insets show a magnified view of the change classes only. (For interpretation of the references to colour in this figure legend, the reader is referred to the web version of this article.)

**Table 8**
Confusion matrix expressed in proportions, accuracies, unbiased area estimates and uncertainty of area estimates, after combining the degradation classes (deg: degradation class, which combines degradation with recovery and degradation with non-recovery).

| | Reference class | | | | | | |
|---|---|---|---|---|---|---|---|
| Map strata | defor | deg | st_forest | non_forest | Total | User's accuracy | Producer's accuracy |
| defor | 0.002 | 0.000 | 0.000 | 0.001 | 0.003 | 0.517 | 0.709 |
| defor_buffer | 0.000 | 0.002 | 0.002 | 0.005 | 0.009 | | |
| deg | 0.000 | 0.042 | 0.017 | 0.002 | 0.061 | 0.692 | 0.827 |
| pos_deg | 0.001 | 0.002 | 0.025 | 0.001 | 0.029 | | |
| st_forest | 0.000 | 0.004 | 0.334 | 0.011 | 0.349 | 0.957 | 0.837 |
| non_forest | 0.000 | 0.000 | 0.022 | 0.527 | 0.548 | 0.96 | 0.962 |
| Total | 0.002 | 0.051 | 0.400 | 0.547 | 1.000 | | |
| Area Estimates ($km^2$) | 157.582 | 3541.406 | 27,841.814 | 38,115.218 | | Overall accuracy: 0.905 | |
| 1.96 × (area std error) | 98.262 | 556.344 | 945.832 | 804.647 | | | |
| Margin of error | 0.624 | 0.157 | 0.034 | 0.021 | | | |

Furthermore, degradation with recovery has high producer's accuracy but low users' accuracy due to confusion between degradation with recovery and degradation without recovery. All area estimates were significantly different from zero with margins of errors <100%. Even the area of deforestation which was estimated at only 0.3% for the entire study period was significantly different from zero. The areas of degradation with and degradation without recovery were estimated with 35% and 26% margins of errors. The mapped area of deforestation, stable forest and non-forest were within the 95% confidence interval of the estimated area (Fig. 18).

Because of confusion between the two degradation classes (degradation with recovery and degradation without recovery), we merged

**Table 9**
Confusion matrix expressed in proportions, accuracies, unbiased area estimates and uncertainty of area estimates, after combining disturbance classes (dis: disturbance class, which combines deforestation, degradation with recovery and degradation with non-recovery).

| | Reference class | | | | | |
|---|---|---|---|---|---|---|
| Map strata | dis | st_forest | non_forest | Total | User's accuracy | Producer's accuracy |
| dis | 0.044 | 0.017 | 0.003 | 0.064 | 0.688 | 0.828 |
| defor_buffer | 0.002 | 0.002 | 0.005 | 0.009 | | |
| pos_deg | 0.003 | 0.025 | 0.001 | 0.029 | | |
| st_forest | 0.004 | 0.334 | 0.011 | 0.349 | 0.957 | 0.837 |
| non_forest | 0.000 | 0.022 | 0.527 | 0.548 | 0.96 | 0.962 |
| Total | 0.053 | 0.4 | 0.547 | 1.000 | | |
| Area estimates ($km^2$) | 3698.989 | 27,841.814 | 38,115.218 | | Overall accuracy: 0.905 | |
| 1.96 × (area std error) | 524.126 | 922.678 | 805.632 | | | |
| Margin of error | 0.142 | 0.033 | 0.021 | | | |

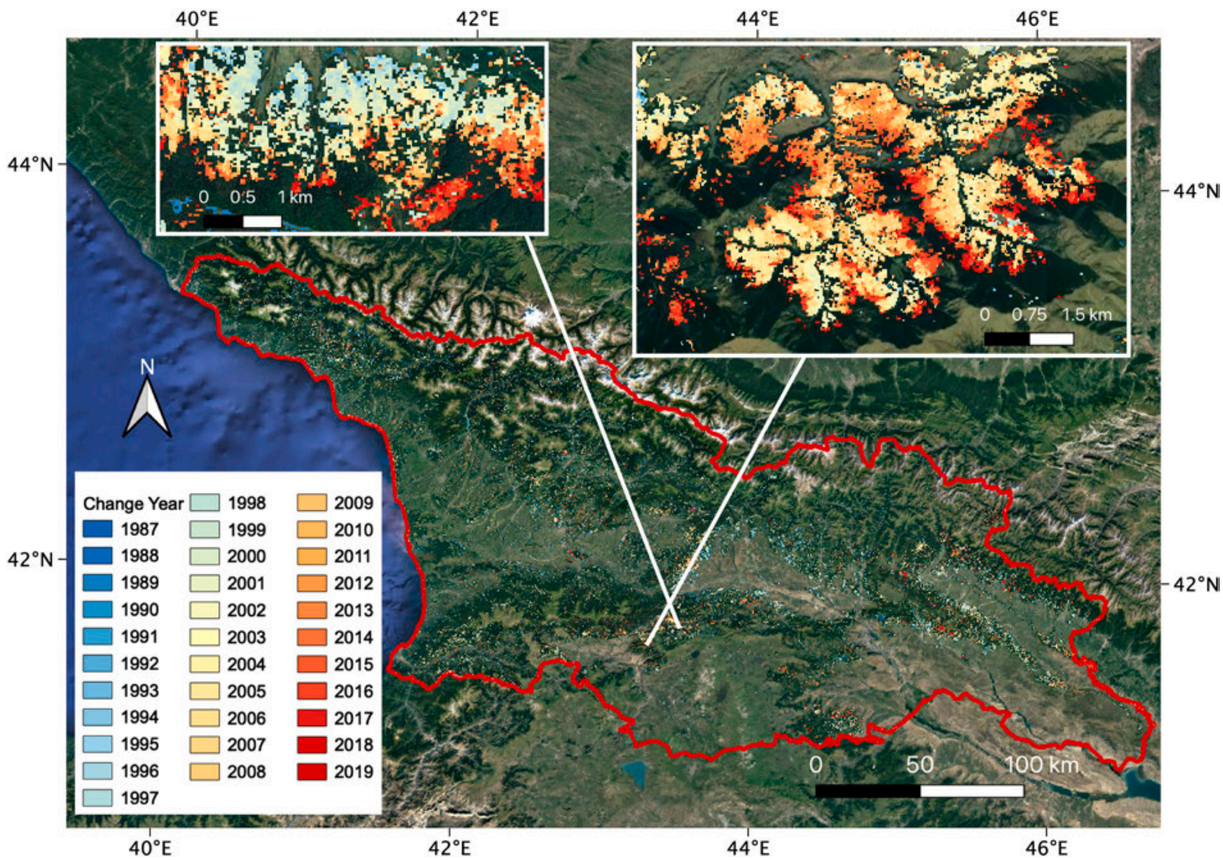


**Fig. 19.** Map of the first year of forest degradation in Georgia. The two insets show expansion of forest degradation in two regions.

them into a single degradation class (Table 8). After merging these two classes, the producer's accuracy and user's accuracy of the degradation class were 83% and 69%, respectively, which was considerably higher and more balanced than the unmerged degradation classes (Table 7). With a single forest degradation class, the overall accuracy of the map increased to 91%. The area estimate of forest degradation with a 95% confidence interval was 3541 $\pm$ 556 $km^2$ (5.08% $\pm$ 0.80% of the study area), equivalent to a margin of error of 16%. The mapped areas based on pixel-counting of the forest degradation were slightly higher than the unbiased area estimates (Fig. 18).

Furthermore, because deforestation and forest degradation are both forest disturbances, we also merged deforestation and forest degradation into a single forest disturbance class. The overall accuracy remains the same, 91%, with user's accuracy and producer's accuracy of the forest disturbance class of 69% and 83%, respectively (Table 9). The 95% confidence interval of the area estimate of the disturbance class was 3698 $\pm$ 524 $km^2$ (5.31% $\pm$ 0.75%) of the study area with 14% margin of error. The mapped areas based on pixel-counting of the forest

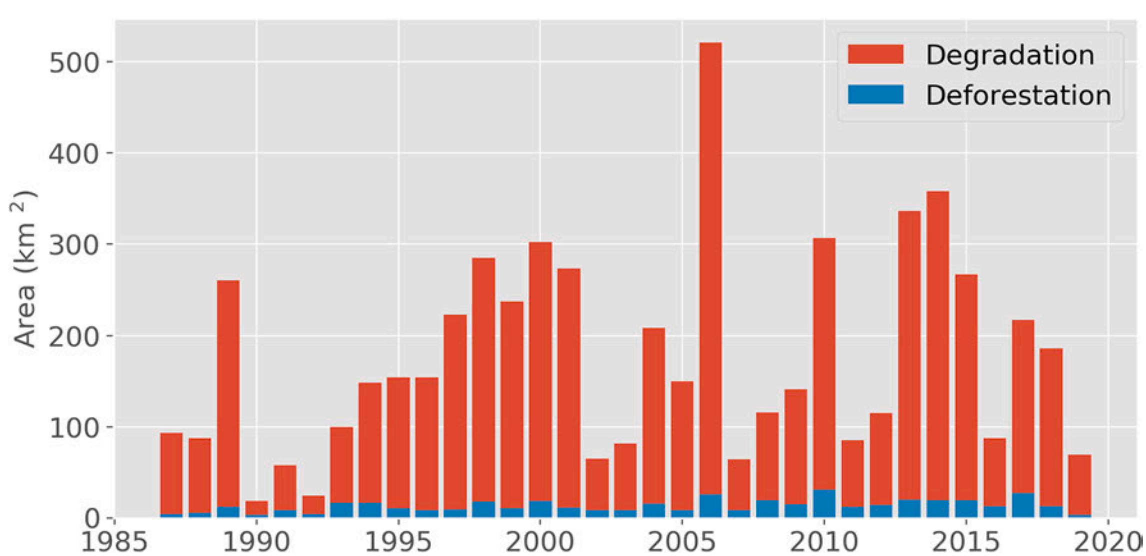


**Fig. 20.** Annual area estimates based on pixel-counting from the map of deforestation and forest degradation from 1987 to 2019. Each time of abrupt degradation was counted in if multiple degradation events occurred, and only the starting year of gradual degradation was counted in.

disturbance classes were slightly higher than the unbiased area estimates (Fig. 18).

We found that the pattern of expansion of forest degradation from more accessible places (close to road and low elevation) to less accessible places (far away from the road and high elevation) was common in some regions in Georgia (insets in Fig. 19). We also found that in total, only 2.3% (99.1 km$^2$; 0.14% of the study area) of the mapped area of forest degradationwas gradual degradation, and thus we did not estimate the unbiased area of gradual degradation separately. Instead, gradual and abrupt degradation were combined into one stratum. Furthermore, the area of degradation increased almost every year from 1992 to 1998 (Fig. 20), might due to an increase in fuelwood and timber demand since energy and timber supply from Soviet Union to Georgia decreased after the collapse of the Soviet Union. Forest degradation in Georgia remains a problem in recent years (Fig. 20).

## 5. Discussion

### 5.1. Evaluation with field conditions

To compare the time series and our map with field conditions, we visited several sites that were mapped as forest degradation around Tbilisi and in the Borjomi region in Georgia in the summer of 2019. In the Borjomi region, forest degradation was prevalent as evident by the presence of stumps, woody debris, branches, or dead trees, in most of the field sites mapped as forest degradation. We compared the time series and the forest conditions in the field. Fig. 21 shows the time series of NDFI and field photos of four field sites. Fig. 21(a) shows an example of a forest that experienced a degradation event in the late 1990s according to the CCDC-SMA algorithm. The field site contains highly rotten stumps, which suggests selective logging occurred about 20–25 years

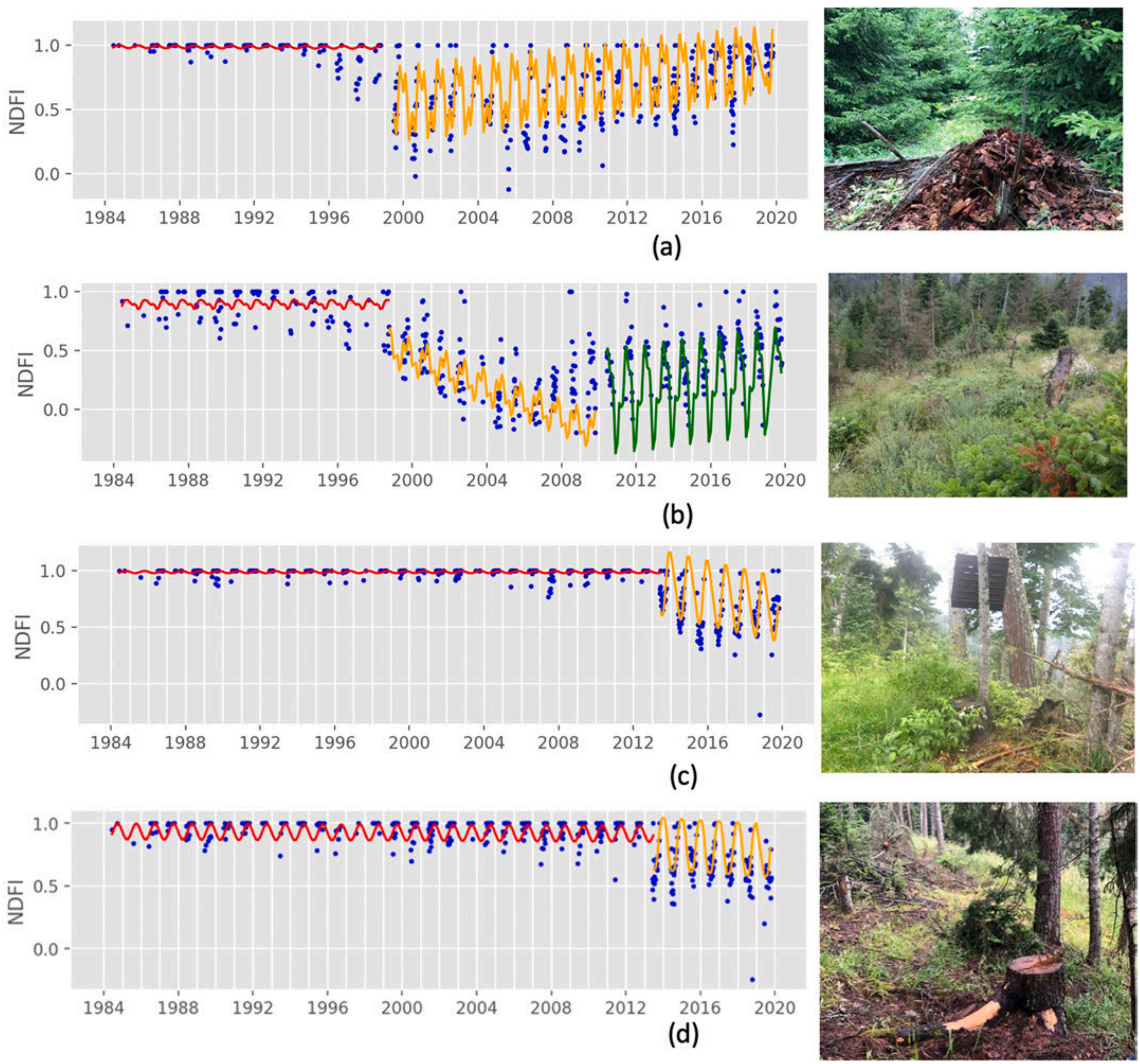


**Fig. 21.** Time series of NDFI and corresponding field photos of: (a) old forest degradation; (b) old illegal logging with some regeneration; (c) pest damage and sanitary cuts; and (d) recent illegal logging. Blue points are observations and colored lines are segments in the time series plots. (For interpretation of the references to colour in this figure legend, the reader is referred to the web version of this article.)

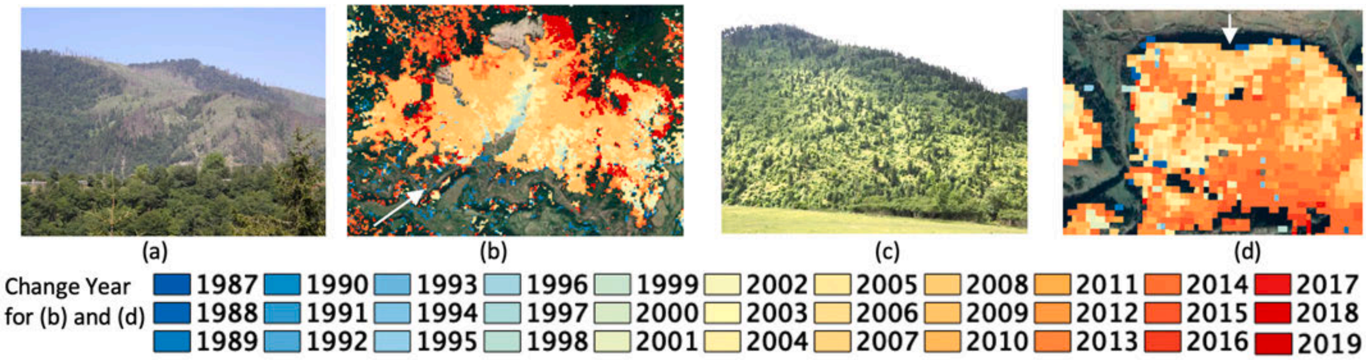


**Fig. 22.** Field photo and year of change map comparison for (a) post-fire forest region; (b) corresponding map of (a); (c) a degraded forest landscape caused by illegal logging; (d) corresponding map of (c). The white arrow shows the directions of where photos were taken from.

ago. Fig. 21(b) shows an example of a forest that experienced gradual degradation from the late 1990s to the late 2000s. This gradual degradation process was caused by continuous extraction of individual trees, as stumps with different degrees of decay were found in the field. As a result of continuous tree removal, large gaps were created, which allowed the understory vegetation to grow. The positive slope of the third time series segment (green line) shows regeneration. Fig. 21(c) and (d) show two examples of more recent degradation. Fig. 21(c) shows pest damage followed by sanitary logging (the black box is an insect trapper). Based on the time series, the degradation event occurred in 2013, which is consistent with the field condition with fresh stumps and branches from legal sanitary cuts. Fig. 21(d) shows an example of recent illegal logging as evident by the relatively fresh stump. Judging from the time series, the degradation event occurred in 2013 and the forest is still not showing any signs of recovery.

We also compared our map of disturbance year with field conditions. Fig. 22(a) shows an area that experienced a forest fire that occurred during the Russo-Georgian War in 2008 and recent degradation at the edge of the post-fire region, which aligns with our map of disturbance year (Fig. 22(b)). Fig. 22(c) shows a mountain with degraded forest as a result of illegal logging that occurred around 2005–2013, which was correctly represented by our map of disturbance year. The recovery of shrubs in Fig. 22(c) indicates that degradation in this area occurred a while ago. In summary, our fieldwork indicates that our map is a good representation of field conditions in the sites we visited. However, since the number of field sites is limited and the locations of field sites is not random or systematic, it is hard to conduct rigorous accuracy assessment using the field data alone.

### *5.2. Comparison with other studies*

Based on our knowledge, there are no official forest degradation statistics or map products for Georgia. Several studies mapped deforestation or forest loss in Georgia, though: Olofsson et al. (2010), using a traditional change detection approach with a limited number of Landsat images, found that 0.8% of forest cover was lost between 1990 and 2000 (0.3% of the country), but this estimate was highly uncertain with an almost 100% margin of error. The global forest cover change dataset produced by Hansen et al. (2013) shows that the area of forest loss from 2000 to 2017 was 799.62 $km^2$ in Georgia (1.15% of the country). Buchner et al. (2020) mapped forest loss and gain from 1987 to 2015 for the Caucasus region for 5-year intervals, including Georgia and found that forest loss in Georgia was miniscule. Our study found that the area of deforestation was very small ($158 \pm 98$ $km^2$ over more than 30 years), which is consistent with those previous studies. No previous study has attempted to estimate forest degradation in Georgia directly. Our study, however, estimated the area of forest degradation in Georgia which was previously understudied and found that forest degradation is the major forest disturbance in Georgia instead of deforestation.

Most forest degradation studies outside of Georgia are in the tropics. Souza et al. (2005) and Souza et al. (2013) applied spectral mixture analysis to map deforestation and forest degradation in Brazil. Bullock et al. (2020b) monitor forest degradation and deforestation in the Amazon region. Schultz et al. (2018) and Hirschmugl et al. (2013) conducted regional studies of monitoring forest degradation in Africa. The accuracy and uncertainty of forest degradation class are comparable with these studies in the tropics. The user's accuracy and producer's accuracy of our degradation class were 69% and 83%, respectively, which is comparable to the accuracy of the study in the Brazilian State of Rondônia (88% for user's accuracy and 68% for producer's accuracy (Bullock et al., 2020a)) and the accuracy of the study in the whole Amazon region (73% for user's accuracy and 44% for producer's accuracy (Bullock et al., 2020b)). Also, the margin of error of our degradation class was 16%, which is comparable with the margins of error in the Amazon studies (Bullock et al. (2020a) and Bullock et al. (2020b), with 14% and 11%, respectively).

### *5.3. Omission errors and commission errors*

All omission errors and commission errors of the degradation class occurred in deciduous forests. We believe that mapped degradation in deciduous forests was less accurate than in coniferous forests since the larger seasonality of deciduous forests makes model fitting of annual spectral variability more challenging than coniferous forests. In addition, deciduous forests cover a larger area than coniferous forests, which may also explain why samples of errors are all in deciduous forests. Omission errors, defined as sample units observed as disturbance in the reference data but occurred in other strata, introduce considerable uncertainty in sampling-based area estimates especially in situations where the area of intact forest is large relative to the area of forest disturbance (Olofsson et al., 2020). Thus, investigating the omission errors would help us to improve the map accuracy and area estimates in the future research. We found two types of omission errors. The first type is that the algorithm detected a break, but the change magnitude was lower than the detection threshold. Fig. 23 shows an example of a forest disturbance event in 2003 that was omitted in the map. A model break was detected in 2003, but because ($M_{soil}$ - $M_{NDFI}$ - $M_{GV}$) was lower than the detection threshold, the event was not identified as a disturbance. The second type of omission error is the result of the algorithm not detecting breaks in the time series. Fig. 24 shows an example of an abrupt degradation event in 1992 that was omitted by the algorithm. This type of error is more complicated to correct. 69% of omission errors fall into the first type, and 31% of omission errors belong to the second type.

Commission errors of forest disturbance carry smaller area weights than omission errors because they occur in the disturbance strata which have smaller area weights than the stable strata, but they also introduce bias and uncertainty both in the map and area estimates. Fig. 25 shows an example of commission error. The density of observations is low in

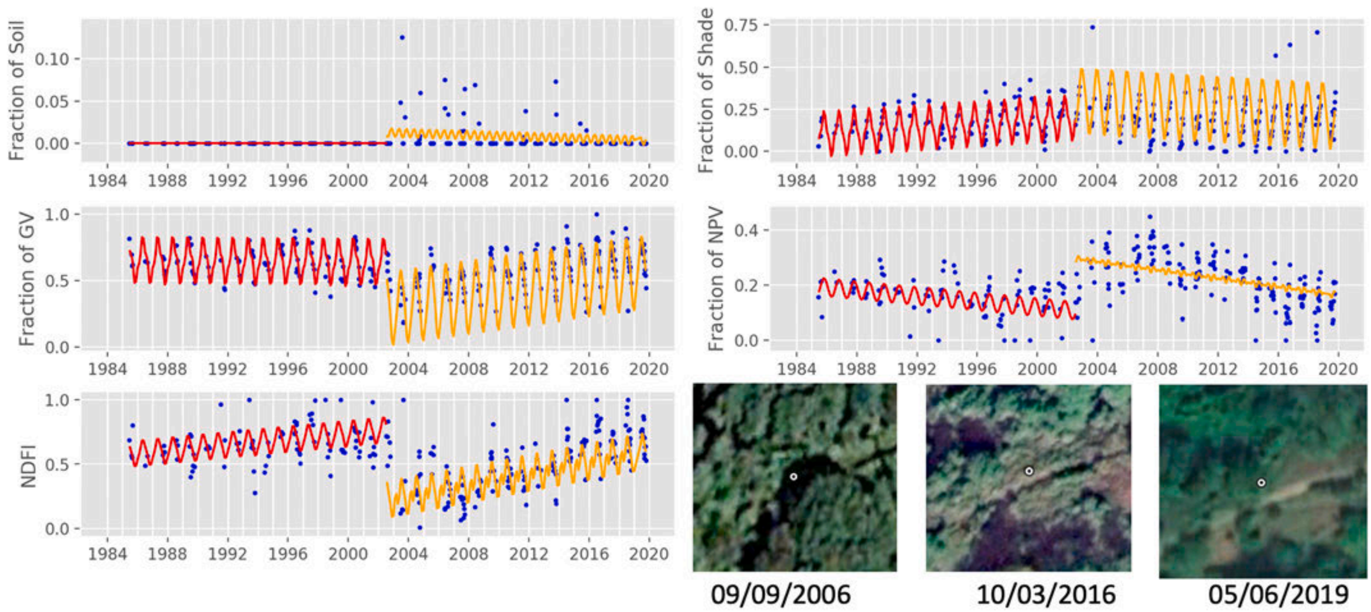


**Fig. 23.** An example of the first type of omission errors. The CCDC-SMA model found a break in 2003, but the break was not identified as forest degradation by the algorithm. The blue points are observations, and the colored lines show different temporal segments. (For interpretation of the references to colour in this figure legend, the reader is referred to the web version of this article.)

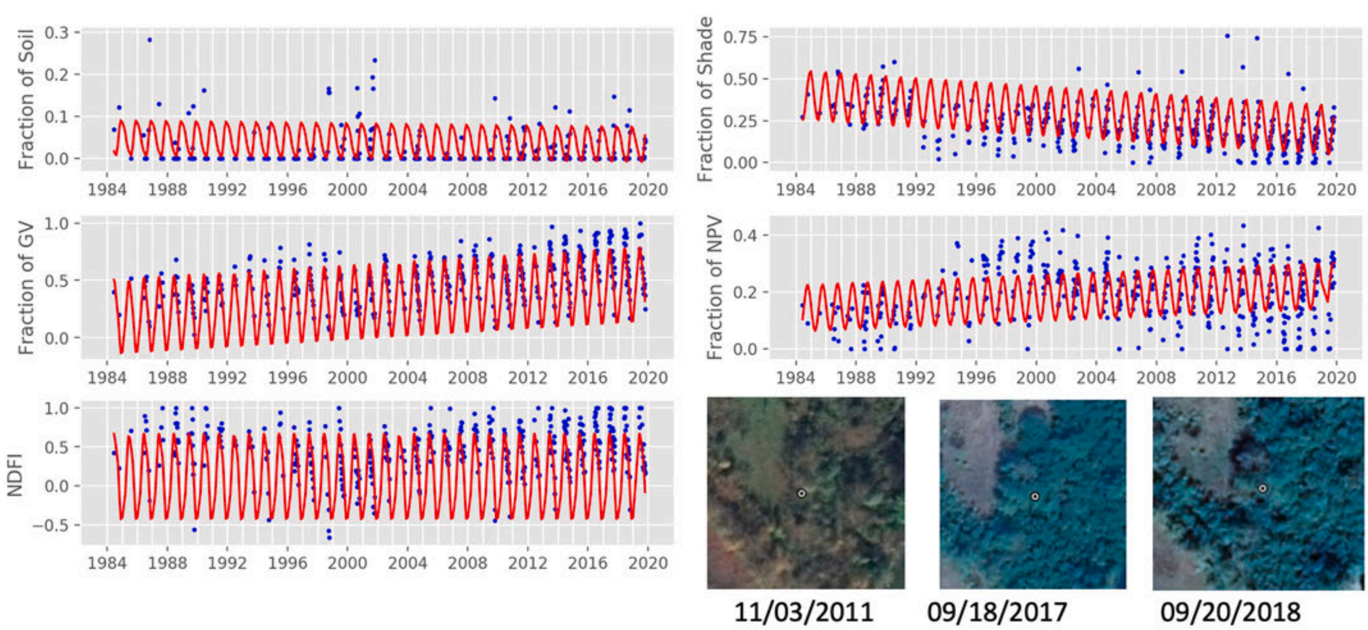


**Fig. 24.** An example of the second type of omission errors. An abrupt degradation event occurred in 1992, but the CCDC-SMA model did not detect the break in 1992. The blue points show observations, and the red line shows the segment. (For interpretation of the references to colour in this figure legend, the reader is referred to the web version of this article.)

the beginning of the time series, which results in a poor model fit. When the data density increases, the model identifies a break instead of updating the first model. When monitoring land cover change, the situation in Fig. 25 would not result in a commission error since both segments are classified as forest, whereas it is considered as a commission error here in forest degradation monitoring. Future study can explore whether fitting the CCDC model from the end of the time series to the start of the time series could solve this problem, since the data density at the end of the time series is usually higher than those in the beginning.

### 5.4. Limitations and future research

There are several limitations of our study which can be improved in the future. First, our study did not distinguish anthropogenic degradation from natural degradation and characterize the severity of forest degradation, which is a limitation for policy making. To gain a comprehensive understanding of the causes of the forest degradation in Georgia, the products and results should be integrated with climatic data, social-economic statistics, and field inventory data (if available in the future) to conduct spatial-temporal causal inference analysis. Further research should explore how to separate anthropogenic causes

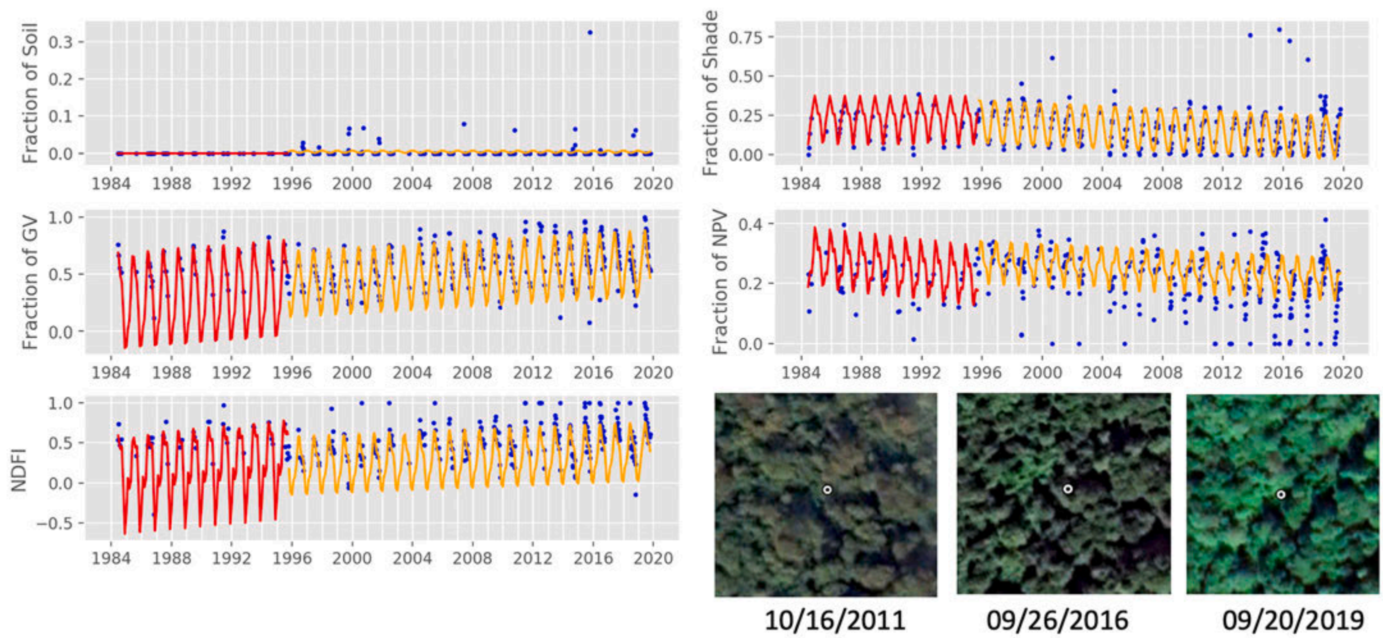


**Fig. 25.** An example of commission error. The pixel is stable forest but mapped as forest degradation. The blue points are observations, and the colored lines show different temporal segments. (For interpretation of the references to colour in this figure legend, the reader is referred to the web version of this article.)

from natural causes and characterize the severity of forest degradation. Second, this study focused on detection of degradation but did not characterize post-degradation status well. Future research should improve characterization of post-degradation status. Third, although we found examples of gradual degradation and developed a method for monitoring it, this process only occurs in a very small area in Georgia, mostly scattered in the Borjomi district. Further studies should explore whether our method works well in places where gradual degradation is prevalent. Fourth, although we compared the time series with field conditions, we were not able to collect enough field data for comprehensive analysis of the relationship between field measurements and remote sensing indices. Georgia is conducting a comprehensive national forest inventory and expected to finish the survey in 2021. In the future, field inventory data can be used to assess the quality of the map and estimate the severity level of degradation. Fifth, this study only used Landsat data to monitor forest degradation. The records of Sentinel and Planet data are growing rapidly, and the data is becoming increasingly available. Future research can explore whether these data could be fused with Landsat data to provide more accurate, robust, and timely monitoring of forest degradation. Last but not least, forest changes, especially forest degradation in the Caucasus Ecoregion are understudied and require more attention. Future research can apply our method to a larger area, such as the Caucasus Ecoregion to explore whether the method is still effective.

## 6. Conclusions

In this study, we developed an approach, CCDC-SMA, to monitor abrupt and gradual degradation in temperate forests. CCDC-SMA runs on Google Earth Engine without the need to download data and can be easily adjusted and applied to other regions. We found that fraction of GV and shade performed differently in response to degradation of different types of forest (deciduous and coniferous), whereas NDFI and fraction of soil performed more consistently. Based on our analysis, using different metrics for monitoring degradation in different forest types can improve the accuracy. The overall accuracy of our map of forest degradation, deforestation, stable forest and non-forest was 91%. The user's accuracy and producer's accuracies of the degradation class were 69% and 83%, respectively. The margin of errors of the estimated area of degradation was 16%. The sampling-based area estimate with 95% confidence intervals of forest degradation was 3541 ± 556 km$^2$, which is significantly larger than the estimated area of deforestation, 158 ± 98 km$^2$. We successfully mapped forest degradation with good accuracy in the country of Georgia, which a previous study failed to map (Olofsson et al., 2010). The accuracy of our results and uncertainty of our area estimates are comparable with other studies in the tropical forests and indicate that Landsat data can be effectively used to map the partial loss of canopy cover associated with forest degradation in temperate regions. Future research can compare the remote sensing products and field inventory data and expand this approach to a larger region.

## Description of author's responsibilities

**Shijuan Chen**: Conceptualization, Data curation, Formal analysis, Methodology, Software, Validation, Visualization, Writing - original draft, Writing - review & editing. **Curtis E. Woodcock**: Conceptualization, Supervision, Resources, Writing - review & editing. **Eric L. Bullock**: Software, Writing - review & editing. **Paulo Arévalo**: Software, Writing - review & editing. **Paata Torchinava**: Resources, Writing - review & editing. **Siqi Peng**: Validation, Writing - review & editing. **Pontus Olofsson**: Conceptualization, Supervision, Funding acquisition, Project administration, Writing - review & editing.

## Declaration of Competing Interest

The authors declare that they have no known competing financial interests or personal relationships that could have appeared to influence the work reported in this paper.

## Acknowledgements

This research was funded by support from the NASA Land-Cover and Land-Use Change Program (grant number: 80NSSC18K0315) to Boston University (PI: Pontus Olofsson) and USGS Landsat Science Team Program for Better Use of the Landsat Temporal Domain: Monitoring Land Cover Type, Condition and Change (grant number: G12PC00070) (PI: Curtis Woodcock). Finally, the authors are grateful to the editors and three anonymous reviewers for their insightful and constructive comments, which greatly helped to improve this paper.

## References


Arévalo, P., Bullock, E.L., Woodcock, C.E., Olofsson, P., 2020. A suite of tools for continuous land change monitoring in Google Earth Engine. Front. Clim. 2, 1–19.

Baccini, A., Walker, W., Carvalho, L., Farina, M., Houghton, R.A., 2017. Tropical forests are a net carbon source based on aboveground measurements of gain and loss. Science 358 (6360), 230–234.

Baumann, M., Ozdogan, M., Kuemmerle, T., Wendland, K.J., Esipova, E., Radeloff, V.C., 2012. Using the Landsat record to detect forest-cover changes during and after the collapse of the Soviet Union in the temperate zone of European Russia. Remote Sens. Environ. 124, 174–184. https://doi.org/10.1016/j.rse.2012.05.001.

Buchner, J., Yin, H., Frantz, D., Kuemmerle, T., Askerov, E., Bakuradze, T., Bleyhl, B., Radeloff, V.C., 2020. Land-cover change in the Caucasus Mountains since 1987 based on the topographic correction of multi-temporal Landsat composites. Remote Sens. Environ. 248, 111967. https://doi.org/10.1016/j.rse.2020.111967.

Bullock, E.L., Woodcock, C.E., Olofsson, P., 2020a. Monitoring tropical forest degradation using spectral unmixing and Landsat time series analysis. Remote Sens. Environ. 238, 110968. https://doi.org/10.1016/j.rse.2018.11.011.

Bullock, E.L., Woodcock, C.E., Souza, C., Olofsson, P., 2020b. Satellite-based estimates reveal widespread forest degradation in the Amazon. Glob. Chang. Biol. 2956–2969 https://doi.org/10.1111/gcb.15029.

Bziava, K., Gubeladze, D., 2003. Georgia's forestry sector: current problems and ways forward. World For. Congr. 1–8.

Casella, G., Berger, R.L., 2002. Statistical Inference, 2nd ed. Duxbury Press, Pacific Grove, CA, p. 330.

Ceccherini, G., Duveiller, G., Grassi, G., Lemoine, G., Avitabile, V., Pilli, R., Cescatti, A., 2020. Abrupt increase in harvested forest area over Europe after 2015. Nature 583, 72–77. https://doi.org/10.1038/s41586-020-2438-y.

Cochran, W.G., 1977. Sampling Techniques, 3rd edition. John Wiley & Sons, New York.

Dalgleish, T., Williams, J.M.G., Golden, A.-M.J., Perkins, N., Barrett, L.F., Barnard, P.J., Au Yeung, C., Murphy, V., Elward, R., Tchanturia, K., Watkins, E., 2007. National forest concept for Georgia. J. Exp. Psychol. Gen. 136, 23–42.

FAO, 2012. Forest Resources Assessment 2015: Terms and Definitions. Forest Resources Assessment (FRA) Working Paper No. 180. Food and Agriculture Organization of the United Nations. Rome, FAO.

FAO, 2015. Global Forest Resources Assessment 2015: How are the World's Forests Changing? Food and Agriculture Organization of the United Nations and European Commission Joint Research Centre. Rome, FAO https://doi.org/10.1002/2014GB005021.

FAO, 2019. State of Forests of the Caucasus and Central Asia. United Nations Economic Commission for Europe (UNECE) and Food and Agriculture Organization of the United Nations (FAO), New York and Geneva.

FAO, 2020a. Global Forest Resources Assessment 2020, Country Report of Georgia. Food and Agriculture Organization of the United Nations, Rome.

FAO, 2020b. Global Forest Resource Assessment 2020, Main Report. Food and Agriculture Organization of the United Nations, Rome. https://doi.org/10.4060/ca9825en.

FAO & JRC, 2012. Global Forest Land-Use Change 1990–2005. FAO Forestry Paper No. 169. Food and Agriculture Organization of the United Nations and European Commission Joint Research Centre. Rome, FAO.

Federici, S., Tubiello, F.N., Salvatore, M., Jacobs, H., Schmidhuber, J., 2015. New estimates of $CO_2$ forest emissions and removals: 1990-2015. For. Ecol. Manag. 352, 89–98. https://doi.org/10.1016/j.foreco.2015.04.022.

Forestry Department at the Georgian Ministry of Environment and Agriculture, 2006. Yearbook of Forestry. The Republic of Georgia, Tbilisi.

Garforth, M., Nilsson, S., Torchinava, P., 2016. Wood Market Study – Final Report. Integrated Biodiversity Management – South Caucasus. GIZ (Consultant report by GFA Consulting Group).

Gorelick, N., Hancher, M., Dixon, M., Ilyushchenko, S., Thau, D., Moore, R., 2017. Google Earth Engine: planetary-scale geospatial analysis for everyone. Remote Sens. Environ. 202, 18–27. https://doi.org/10.1016/j.rse.2017.06.031.

Gutman, G., Radeloff, V., 2016. Land-Cover and Land-Use Changes in Eastern Europe after the Collapse of the Soviet Union in 1991. https://doi.org/10.1007/978-3-319-42638-9.

Hansen, M.C., Potapov, P.V., Moore, R., Hancher, M., Turubanova, S.A.A., Tyukavina, A., Kommareddy, A., 2013. High-resolution global maps of 21st-century forest cover change. Science 342, 850–853. https://doi.org/10.1126/science.1244693.

Herold, M., Avitabile, V., Román-Cuesta, R.M., Mollicone, D., Hirata, Y., Van Laake, P., Asner, G.P., Souza, C., Skutsch, M., MacDicken, K., 2011. Options for monitoring and estimating historical carbon emissions from forest degradation in the context of REDD+. Carbon Balance Manag. 6, 1–7. https://doi.org/10.1186/1750-0680-6-13.

Hirschmugl, M., Steinegger, M., Gallaun, H., Schardt, M., 2013. Mapping forest degradation due to selective logging by means of time series analysis: Case studies in Central Africa. Remote Sens. 6, 756–775. https://doi.org/10.3390/rs6010756.

IPCC, 2003. Definitions and Methodological Options to Inventory Emissions from Direct Human-Induced Degradation of Forests and Devegetation of Other Vegetation Types 3–32.

Kennedy, R.E., Yang, Z., Cohen, W.B., 2010. Detecting trends in forest disturbance and recovery using yearly Landsat time series: 1. LandTrendr - temporal segmentation algorithms. Remote Sens. Environ. 114, 2897–2910. https://doi.org/10.1016/j.rse.2010.07.008.

Kennedy, R.E., Andréfouët, S., Cohen, W.B., Gómez, C., Griffiths, P., Hais, M., Zhu, Z., 2014. Bringing an ecological view of change to landsat-based remote sensing. Front. Ecol. Environ. 12, 339–346. https://doi.org/10.1890/130066.

Krever, V., Zazanashvili, N., Jungius, H., Williams, L., Petelin, D., 2001. Biodiversity of the Caucasus Ecoregion: An Analysis of Biodiversity and Current Threats and Initial Investment Portfolio. World Wide Fund for Nature.

Kuemmerle, T., Olofsson, P., Chaskovskyy, O., Baumann, M., Ostapowicz, K., Woodcock, C.E., Houghton, R.A., Hostert, P., Keeton, W.S., Radeloff, V.C., 2011. Post-Soviet farmland abandonment, forest recovery, and carbon sequestration in western Ukraine. Glob. Chang. Biol. 17, 1335–1349. https://doi.org/10.1111/j.1365-2486.2010.02333.x.

Lewińska, K.E., Hostert, P., Buchner, J., Bleyhl, B., Radeloff, V.C., 2020. Short-term vegetation loss versus decadal degradation of grasslands in the Caucasus based on Cumulative Endmember Fractions. Remote Sens. Environ. 248, 1–21. https://doi.org/10.1016/j.rse.2020.111969.

Matcharashvili, I., 2012. Problems and Challenges of Forest Governance in Georgia. Association Green Alternative, Tbilisi, 38 p.

Matricardi, E., Skole, D.L., Costa, O.B., 2020. Long-term forest degradation surpasses deforestation in the Brazilian Amazon. Science 369 (6509), 1378–1382.

Miettinen, J., Stibig, H.J., Achard, F., 2014. Remote sensing of forest degradation in Southeast Asia-Aiming for a regional view through 5-30 m satellite data. Glob. Ecol. Conserv. 2, 24–36. https://doi.org/10.1016/j.gecco.2014.07.007.

Mitchell, A.L., Rosenqvist, A., Mora, B., 2017. Current remote sensing approaches to monitoring forest degradation in support of countries measurement, reporting and verification (MRV) systems for REDD+. Carbon Balance Manag. 12 https://doi.org/10.1186/s13021-017-0078-9.

Olofsson, P., Torchinava, P., Woodcock, C.E., Baccini, A., Houghton, R.A., 2010. Implications of land use change on the national terrestrial carbon budget of Georgia. Carbon Balance Manag. 5, 4.

Olofsson, P., Kuemmerle, T., Griffiths, P., Knorn, J., Baccini, A., Gancz, V., Blujdea, V., Houghton, R.A., Abrudan, I.V., Woodcock, C.E., 2011. Carbon implications of forest restitution in post-socialist Romania. Environ. Res. Lett. 6 https://doi.org/10.1088/1748-9326/6/4/045202.

Olofsson, P., Foody, G.M., Stehman, S.V., Woodcock, C.E., 2013. Making better use of accuracy data in land change studies: estimating accuracy and area and quantifying uncertainty using stratified estimation. Remote Sens. Environ. 129, 122–131. https://doi.org/10.1016/j.rse.2012.10.031.

Olofsson, P., Foody, G.M., Herold, M., Stehman, S.V., Woodcock, C.E., Wulder, M.A., 2014. Good practices for estimating area and assessing accuracy of land change. Remote Sens. Environ. 148, 42–57. https://doi.org/10.1016/j.rse.2014.02.015.

Olofsson, P., Arévalo, P., Espejo, A.B., Green, C., Lindquist, E., McRoberts, R.E., Sanz, M. J., 2020. Mitigating the effects of omission errors on area and area change estimates. Remote Sens. Environ. 236, 111492. https://doi.org/10.1016/j.rse.2019.111492.

Pearson, T.R.H., Brown, S., Murray, L., Sidman, G., 2017. Greenhouse gas emissions from tropical forest degradation: an underestimated source. Carbon Balance Manag. 12, 3. https://doi.org/10.1186/s13021-017-0072-2.

Potapov, P.V., Turubanova, S.A., Tyukavina, A., Krylov, A.M., McCarty, J.L., Radeloff, V. C., Hansen, M.C., 2015. Eastern Europe's forest cover dynamics from 1985 to 2012 quantified from the full Landsat archive. Remote Sens. Environ. 159, 28–43. https://doi.org/10.1016/j.rse.2014.11.027.

Quintano, C., Fernández-Manso, A., Roberts, D.A., 2013. Multiple Endmember Spectral Mixture Analysis (MESMA) to map burn severity levels from Landsat images in Mediterranean countries. Remote Sens. Environ. 136, 76–88. https://doi.org/10.1016/j.rse.2013.04.017.

Rappaport, D., Morton, D., Longo, M., Keller, M., Dubayah, R., Dos-Santos, M.N., 2018. Quantifying long-term changes in carbon stocks and forest structure from Amazon forest degradation. Environ. Res. Lett. 13 https://doi.org/10.1088/1748-9326/aac331, 065013.

Roy, D.P., Kovalskyy, V., Zhang, H.K., Vermote, E.F., Yan, L., Kumar, S.S., Egorov, A., 2016a. Characterization of Landsat-7 to Landsat-8 reflective wavelength and normalized difference vegetation index continuity. Remote Sens. Environ. 185, 57–70. https://doi.org/10.1016/j.rse.2015.12.024.

Roy, D.P., Zhang, H.K., Ju, J., Gomez-Dans, J.L., Lewis, P.E., Schaaf, C.B., Sun, Q., Li, J., Huang, H., Kovalskyy, V., 2016b. A general method to normalize Landsat reflectance data to nadir BRDF adjusted reflectance. Remote Sens. Environ. 176, 255–271. https://doi.org/10.1016/j.rse.2016.01.023.

Schultz, M., Shapiro, A., Clevers, J.G.P.W., Beech, C., Herold, M., 2018. Forest cover and vegetation degradation detection in the Kavango Zambezi Transfrontier Conservation area using BFAST monitor. Remote Sens. 10 https://doi.org/10.3390/rs10111850.

Simula, M., 2009. Towards Defining Forest Degradation: Comparative Analysis of Existing Definitions. Forest Resources Assessment Working Paper.

Souza, C.M., Roberts, D.A., Cochrane, M.A., 2005. Combining spectral and spatial information to map canopy damage from selective logging and forest fires. Remote Sens. Environ. 98, 329–343. https://doi.org/10.1016/j.rse.2005.07.013.

Souza, C.M., Siqueira, J.V., Sales, M.H., Fonseca, A.V., Ribeiro, J.G., Numata, I., Cochrane, M.A., Barber, C.P., Roberts, D.A., Barlow, J., 2013. Ten-year Landsat classification of deforestation and forest degradation in the Brazilian Amazon. Remote Sens. 5, 5493–5513. https://doi.org/10.3390/rs5115493.

Strahler, A., 2011. Introducing Physical Geography. John Wiley & Sons, Inc. Chapter 7, pp. 216–263.

Verbesselt, J., Hyndman, R., Newnham, G., Culvenor, D., 2010. Detecting trend and seasonal changes in satellite image time series. Remote Sens. Environ. 114, 106–115. https://doi.org/10.1016/j.rse.2009.08.014.

Vogelmann, J.E., Gallant, A.L., Shi, H., Zhu, Z., 2016. Perspectives on monitoring gradual change across the continuity of Landsat sensors using time-series data. Remote Sens. Environ. 185, 258–270. https://doi.org/10.1016/j.rse.2016.02.060.

Woodcock, C.E., Allen, R.G., Anderson, M., Belward, A., Bindschadler, R., Cohen, W.B., Wynne, R., 2008. Free access to Landsat imagery. Science 320 (5879), 1011.

World Bank, 2020. South Caucasus: Armenia, Azerbaijan and Georgia: Private Enterprises in the Forest Sector – A Survey of the Private Sector in Wood Production and Processing.

Wulder, M.A., White, J.C., Loveland, T.R., Woodcock, C.E., Belward, A.S., Cohen, W.B., Fosnight, E.A., Shaw, J., Masek, J.G., Roy, D.P., 2016. The global Landsat archive: status, consolidation, and direction. Remote Sens. Environ. 185, 271–283. https://doi.org/10.1016/j.rse.2015.11.032.

Zeidler, U., Schachtschabel, G.D., 2016. Strategic environmental and social assessment of draft Forest Code of Georgia. In: European Neighborhood and Partnership Instrument East Countries Forest Law Enforcement and Governance II Program. https://www.enpi-fleg.org/site/assets/files/2190/act_1_1_sesa_forest_code_georgia_-_final_of_jan_27.pdf.

Zhu, Z., Woodcock, C.E., 2012. Object-based cloud and cloud shadow detection in Landsat imagery. Remote Sens. Environ. 118, 83–94. https://doi.org/10.1016/j.rse.2011.10.028.

Zhu, Z., Woodcock, C.E., 2014a. Automated cloud, cloud shadow, and snow detection in multitemporal Landsat data: An algorithm designed specifically for monitoring land cover change. Remote Sens. Environ. 152, 217–234. https://doi.org/10.1016/j.rse.2014.06.012.

Zhu, Z., Woodcock, C.E., 2014b. Continuous change detection and classification of land cover using all available Landsat data. Remote Sens. Environ. 144, 152–171. https://doi.org/10.1016/j.rse.2014.01.011.

Zhu, Z., Woodcock, C.E., Olofsson, P., 2012. Continuous monitoring of forest disturbance using all available Landsat imagery. Remote Sens. Environ. 122, 75–91. https://doi.org/10.1016/j.rse.2011.10.030.

Zhu, Z., Woodcock, C.E., Holden, C., Yang, Z., 2015. Generating synthetic Landsat images based on all available Landsat data: Predicting Landsat surface reflectance at any given time. Remote Sens. Environ. 162, 67–83. https://doi.org/10.1016/j.rse.2015.02.009.